The Ocean Response to Low-Frequency Interannual Atmospheric Variability in the Mediterranean Sea. Part I: Sensitivity Experiments and Energy Analysis

G. KORRES

Laboratory of Meteorology, Department of Applied Physics, University of Athens, Athens, Greece

N. PINARDI

Istituto di Scienze dell'Atmosfera e dell'Oceano, CNR, Bologna, Italy

A. LASCARATOS

Laboratory of Meteorology, Department of Applied Physics, University of Athens, Athens, Greece

(Manuscript received 18 March 1998, in final form 13 April 1999)

ABSTRACT

In this study a general circulation model is used in order to investigate the interannual response of the Mediterranean Basin to low-frequency interannual variability in atmospheric forcing for the period 1980–88. The model incorporates a realistic scheme for the air–sea interaction physics, has 31 levels in the vertical, and a quarter of a degree horizontal resolution.

The simulations show the strong seasonal and interannual signal of the upper thermocline Mediterranean general circulation. Interannual variability of the basin has an eventlike character (anomalous winter wind curl for 1981 and 1986, heat flux winter anomalies in 1981 and 1987) and it is mainly forced by wintertime anomalies; for example, it is locked to the seasonal cycle. The Ionian and the eastern Levantine areas are found to be more prone to interannual changes. The Gibraltar mass transport undergoes small seasonal changes around an average value of 0.95 Sverdrup (Sv) while the Sicily Strait transport is characterized by much stronger seasonal and interannual fluctuations around an average of 1.5 Sv. Sensitivity experiments to atmospheric forcing show that large anomalies in winter wind events can shift the timing of occurrence of the seasonal cycle. Energy cycles involve exchanges between barotropic, baroclinic kinetic energy, and available potential energy reservoirs. The analysis presented here shows that the direction of conversion between these reservoirs depends on the wind strength. During winter, energy is stored in the available potential energy pool and the kinetic energy is directly forced by winds. During summer kinetic energy grows at the expense of available potential energy following the well-known baroclinic instability conversion process.

1. Introduction

The Mediterranean Basin has received a lot of interest recently since it can be considered as a suitable test basin for understanding some of the processes associated with the oceanic general circulation. A review of the implications of Mediterranean physical oceanography problems in a global context is given by the POEM Group (1992). Naturally the description and understanding of the seasonal and interannual general circulation variabilities are not being adequately addressed by the purely observational evidence due to the lack of high-resolution space–time datasets. Thus there is an unresolved question about the origin and structure of the interannual variability of the basin general circulation that can be addressed by general circulation modeling. In this paper we explore some of the dynamical mechanisms responsible for interannual variability in the Mediterranean Sea with such a general circulation model, focusing on the ocean response to atmospheric forcing.

The first evidence of interannual variability in the water mass properties of the basin is offered by Hecht (1992), who describes a general increase of the salinity in the southeastern part of the eastern Mediterranean (EMED) in 1982–83 with a consequent disappearance of the Levantine Intermediate Water (LIW) subsurface maximum. Furthermore, Robinson et al. (1991) discuss the possibility of ''recurrent'' gyres, for example, gyres that are disappearing and/or appearing from year to year. In the western Mediterranean (WMED) there is a notion of large interannual variability in the rate of formation of western deep waters (WDW) in the Gulf of Lions

Corresponding author address: Dr. Nadia Pinardi, ISAO-CNR, Via Gobetti 101, 40129 Bologna, Italy.
E-mail: n.pinardi@isao.bo.cnr.it

region (Leaman and Schott 1991; Bethoux and Gentili 1996). Millot (1991) discusses the interannual variabilities associated with the eddies of the Algerian current. Astraldi et al. (1994) find interannual variability in the mass transport at the Corsica Strait in the northwestern Mediterranean (see Fig. 1). Roether et al. (1996) documented a spectacular change in water mass properties that occurred between 1987 and 1995 in the eastern Mediterranean due to the outflow of Aegean waters into the abyssal Ionian Basin. Such a change is not considered here mainly due to the time resolution of our dataset and the modeling limitations with respect to the resolution of the outflow from straits and passages. However, our work sets the basis to understand changes in the ocean circulation due to atmospheric forcing that may have created conditions for the deep water mass change to occur.

The Mediterranean Sea is a semienclosed concentration basin (see Fig. 1) extending long 30° $\times$ lat 10°. It is subdivided by the sill of Sicily Strait ($\sim$300 m depth) into the WMED and EMED subbasins. The EMED consists of the Adriatic, Ionian, Aegean, and Levantine Seas, while the WMED is composed by the Alboran, Balearic, Ligurian, and Tyrrhenian Seas. The Mediterranean Sea acts as an engine that, by intense air–sea interactions, transforms the hydrological characteristics of the inflowing Atlantic water (AW) to the temperature–salinity (*T–S*) properties of the outflowing mixture of LIW (the intermediate water mass formed in the Levantine area) and WDW. Two distinct deep water masses are formed, one in the Gulf of Lions area for the WMED and the other in the Adriatic Sea for the EMED.

Basin-, subbasin-scale and mesoscale features are interacting in order to compose the general circulation picture. The recent modeling efforts (Pinardi and Navarra 1993; Malanotte-Rizzoli and Bergamasco 1991; Roussenov et al. 1995; Zavatarelli and Mellor 1995; Herbaut et al. 1996, 1997; Pinardi et al. 1997; Horton et al. 1997) have pointed out both the seasonal and interannual signal of this general circulation. However, none of them concentrated on the study of a long time series of simulated fields in order to understand and describe the causes of the interannual variability. Other studies have elucidated the WDW and LIW formation and spreading processes (Madec et al. 1991; Lascaratos and Nittas 1998; Haines and Wu 1995; Wu and Haines 1996), and others have considered mesoscale dynamics within the larger, wind- and thermohaline-driven flow field (Milliff and Robinson 1992; Robinson and Golnaraghi 1993). These process-oriented studies considered idealized atmospheric forcing or subbasin high-resolution modeling.

The Mediterranean circulation can be thought to be driven by three major external forcing agents: the wind, the inflow/outflow at the Gibraltar Strait, and the buoyancy fluxes at the air–sea interface. The Gibraltar inflow is assumed to be constant here (see model design section) and thus it is not considered as a source of interannual variability for the flow field. On the other hand, wind and thermal flux interannual changes are central to our modeling effort. The water fluxes are considered only to be seasonal due to the lack of reliable precipitation data for the years 1980–88.

Recently Garrett et al. (1993) using a 43-yr time series (1946–88) taken from the Comprehensive Ocean–Atmosphere Data Set (COADS) has shown a large interannual signal of the heat fluxes over the Mediterranean area. Castellari et al. (1998) show the amplitude of the interannual fluctuations in the heat fluxes using the same 9-yr time series of atmospheric parameters that we use in this study. These authors show large interannual anomalies in the sensible and latent heat fluxes fields at the timescale of 5–6 yr. Interannual variations also characterize the momentum fluxes computed from the same time series. Heburn (1994) shows the strong interannual variability of the ocean response using European Centre for Medium-Range Weather Forecasts 1981–89 wind stresses. In particular he points out the large wind curl anomaly occurring during the winter of 1981 affecting mainly the eastern subbasin and which we find also in our dataset.

This paper describes several interannual simulations and sensitivity experiments in order to understand the dynamics of the oceanic response to the low-frequency atmospheric forcing. Along these lines we use the Geophysical Fluid Dynamics Laboratory Modular Ocean Model (Pacanowski et al. 1990) adapted to the Mediterranean Basin by Roussenov et al. (1995). We use the National Centers for Environmental Prediction (NCEP) monthly mean atmospheric analyses at 1000 mb for the 9-yr period 1980–88. In this paper (Part I) we analyze the simulations and carry out sensitivity experiments and energy analyses. In Korres et al. (2000) (Part II) we conclude the analysis of the time and space scales of the variability using empirical orthogonal functions.

In section 2 we give a brief description of the model design and the experiments performed. In section 3 we discuss some of the characteristics of the heat and momentum fields obtained during the model integration. Section 4 deals with the steady-state components of the Mediterranean circulation. In sections 5 and 6 we present and discuss the variability of the upper-thermocline flow fields (at 30 and 300 m) for the winters and summers of 1981, 1984, 1986, and 1987, and we discuss the possible mechanisms responsible for interannual variability. In section 7 we investigate the volume and heat transports at the various straits of the basin. The energetics of the Mediterranean circulation under various types of external forcing are discussed in the section that follows. Finally we intercompare the model dynamic height fields with the observational evidence collected during the Physical Oceanography of the Eastern Mediterranean (POEM) general circulation surveys in section 9. Conclusions are offered in section 10.

2. Model design

The model design utilized in the present work is based upon Roussenov et al. (1995) so we will give here only

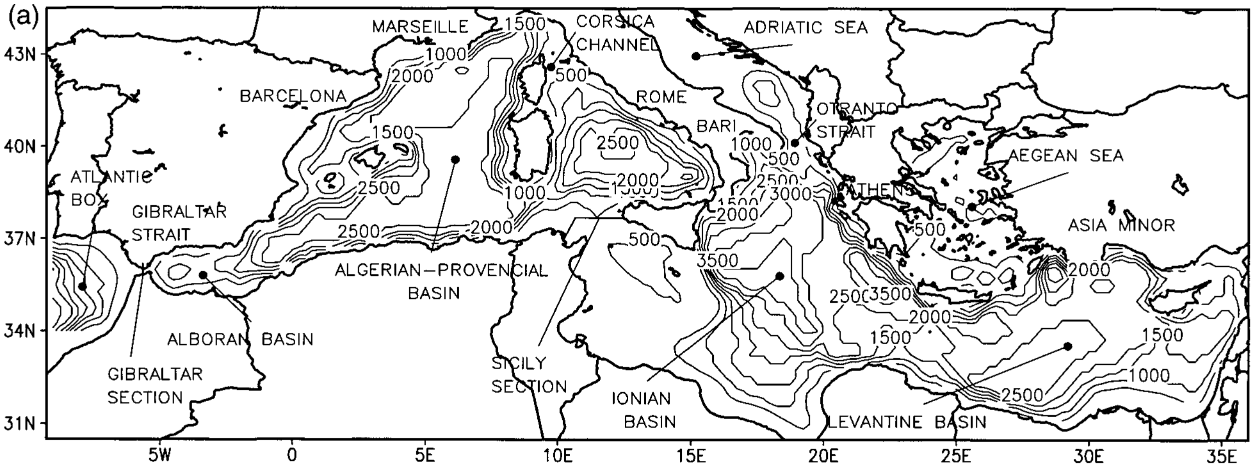

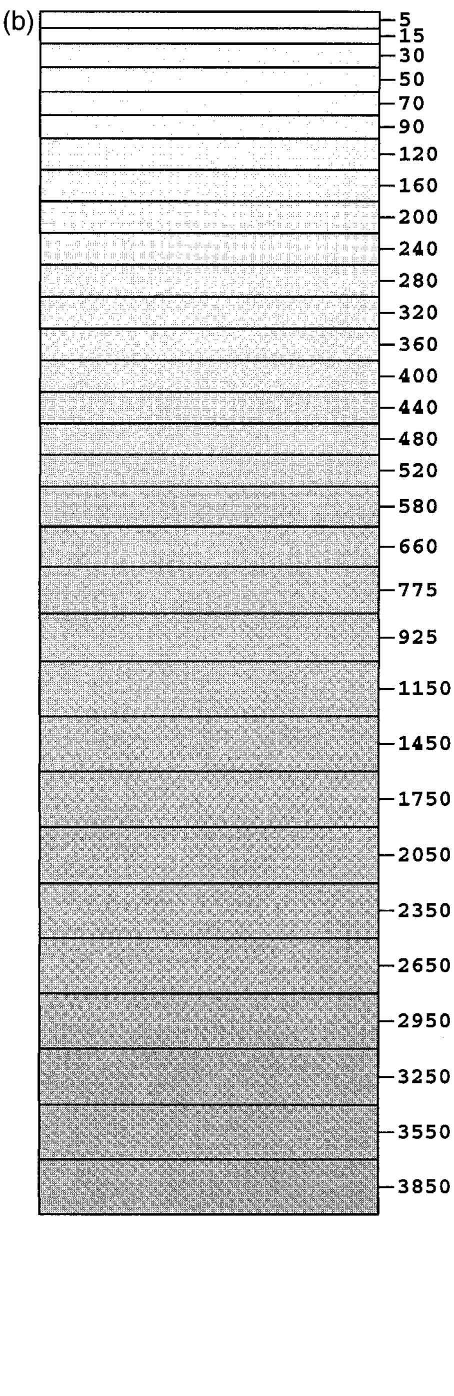

FIG. 1. (a) Model topography (contour interval 250 m). (b) Model-level positions and thicknesses.

a brief description of the basic model features. Our effort improves the previous modeling work of Roussenov et al. (1995) as it incorporates a better resolution in the vertical, a more realistic model initialization, and an implementation of cloud cover data into the heat fluxes parameterization scheme. A noticeable characteristic of the model is the air–sea interaction scheme that includes a sophisticated heat and momentum parameterization at the air–sea interface, as originally used by Rosati and Miyakoda (1988) for the World Ocean. The horizontal resolution of the model is a quarter of a degree in both latitude and longitude, so we do not resolve the Rossby deformation scales, which in the Mediterranean are of the order of 10 km. The model topography including the nomenclature for the main Mediterranean areas is shown in Fig. 1a and has been obtained by a cubic spline interpolation from the U.S. Navy bathymetric $\frac{1}{12}°$ database. We have closely followed the land–sea configuration of Roussenov et al. (1995) with the only exception being the Adriatic Sea, which is more extended to the north. All the main islands are well resolved by the model topography but we have decided to merge together Majorca–Minorca, and Corsica–Sardinia, and connect Sicily and Rhodes with the main land. Also several islands in the Aegean have been connected together for numerical reasons. In Fig. 1b we show the 31 model levels, depths, and thicknesses. The last level is at 3850 m while the resolution varies from 10 m at the surface to 300 m in the deep part of the basin. The upper part of the water column, which includes the AW and LIW layers, is very well resolved by this level distribution.

The model assumes hydrostaticity and the Boussinesq approximation and it is governed by the equations of motion and continuity:

$$\frac{\partial \mathbf{v}_h}{\partial t} + \mathbf{v}_h \cdot \boldsymbol{\nabla}\mathbf{v}_h + w\frac{\partial \mathbf{v}_h}{\partial z} + \mathbf{f}\times\mathbf{v}_h = -\frac{1}{\rho_o}\boldsymbol{\nabla}p + K_m\frac{\partial^2 \mathbf{v}_h}{\partial z^2} + F_m \quad (1)$$

$$\frac{\partial p}{\partial z} = -\rho g \quad (2)$$

$$\boldsymbol{\nabla}\cdot\mathbf{v}_h + \frac{\partial w}{\partial z} = 0. \quad (3)$$

The conservation equations for T and S have the form

$$\frac{\partial T}{\partial t} + \mathbf{v}_h\cdot\boldsymbol{\nabla}T + w\frac{\partial T}{\partial z} + = F_T + K_h\frac{\partial^2 T}{\partial z^2} + \gamma_T(x, y, z)(T^* - T) \quad \text{and} \quad (4)$$

$$\frac{\partial S}{\partial t} + \mathbf{v}_h\cdot\boldsymbol{\nabla}S + w\frac{\partial S}{\partial z} + = F_S + K_h\frac{\partial^2 S}{\partial z^2} + \gamma_S(x, y, z)(S^* - S). \quad (5)$$

The equation of state $\rho = \rho(T, S, p)$ is taken to be a third-order polynomial fit to the UNESCO equation of state.

In the above formulation $\boldsymbol{\nabla}$ is the horizontal gradient operator and $\mathbf{v}_h$ the horizontal velocity vector. We have adopted the scale-selective biharmonic lateral mixing for momentum $F_m = -A_m\nabla^4\mathbf{v}_h$ and tracers $F_T = -A_h\nabla^4 T$, $F_S = -A_h\nabla^4 S$. Horizontal eddy viscosity and eddy diffusivity coefficients are taken to be $A_m = 8 \times 10^{18}$ cm^4 s^{-1} and $A_h = 2.4 \times 10^{19}$ cm^4 s^{-1}. Vertical mixing of tracers depends on the static stability of the water column. Whenever $\partial_z\rho < 0$ (stable conditions), K_h is taken to be equal to 1 cm^2 s^{-1}. In unstable cases the coefficient goes to infinity and the tracers are locally homogenized. For the vertical mixing of momentum we choose $K_m = 1.5$ cm^2 s^{-1}. In order to simulate the inflow/outflow at the Gibraltar Strait we used a buffer zone west of Gibraltar in a 3° × 3° Atlantic box area. There we relax temperature and salinity profiles to the annual mean climatology without imposing any external forcing. In Eqs. (4) and (5) the restoring terms are nonzero only in the Atlantic box area for both tracers and at the surface for salinity only. The restoring timescale ($1/\gamma_T$, $1/\gamma_S$) is set to 5 days.

The model boundary conditions at the sea surface ($z = 0$) are the following.

- The momentum budget takes the form

$$\rho_o A_m\frac{\partial \mathbf{v}_h}{\partial z} = \boldsymbol{\tau}, \quad (6)$$

where $\boldsymbol{\tau} = \rho_a C_D|\mathbf{W}|\mathbf{W}$ with $\mathbf{W}$ being the monthly mean 1000-mb wind vector. The model calculates the drag coefficient C_D using the polynomial approximation of Hellerman and Rosenstein (1983) using air and ocean temperatures and the strength of the wind forcing.

- For the heat budget we assume

$$\rho_o C_p K_h\frac{\partial T}{\partial z} = Q_T = Q_s - Q_u, \quad (7)$$

where Q_T is the net heat flux. In (7) Q_s is the downward flux of solar radiation and Q_u is the net upward heat flux. The model calculates Q_s through the expression

$$Q_s = Q_0(1 - 0.62C + 0.0019\beta)(1 - \alpha), \quad (8)$$

where the different symbols in (8) are explained in Table 1. The net upward flux Q_u is given by the formula

$$Q_u = Q_B + H_a + LE, \quad (9)$$

where Q_B is the longwave back radiation,

$$Q_B = \epsilon\sigma T_s^4[0.39 - 0.05 r_h e_{\text{sat}}^{1/2}(T_a)] + 4\epsilon\sigma T_s^3(T_s - T_a);$$

H_a is the sensible heat flux,

$$H_a = \rho_a C_p C_h|\mathbf{W}|(T_s - T_a);$$

TABLE 1. List of symbols and their meanings for (7), (8), and (9).

Symbol	Meaning and value
Q_0	Total radiation reaching the sea surface under clear sky conditions (Rosati and Miyakoda 1988)
α	Albedo (0.03)
β	Solar noon altitude (Rosati and Miyakoda 1988)
ϵ	Emissivity of the sea
σ	Stefan–Boltzmann constant
r_h	Monthly mean relative humidity at 1000 mb
$e_{\text{sat}}(T)$	Polynomial approximation to the saturation water pressure as given by Lowe (1977)
ρ_a	Density of the air
p_a	Surface air pressure (1013 mb)
C_p	Specific heat capacity (1.005×10^3 J kg^{-1} K^{-1})
C_h, C_e	Turbulent exchange coefficients (1.1×10^3)
C	Monthly mean cloud cover
L	Latent heat of vaporization (2.501×10^6 J kg^{-1})
T_s	Sea surface temperature
T_a	Monthly mean atmospheric temperature at 1000 mb
ρ_0	Seawater density

E is the latent heat flux,

$$E = \rho_a C_e |\mathbf{W}| [e_{\text{sat}}(T_s) - r_h e_{\text{sat}}(T_a)](0.622/p_a);$$

and all the different symbols in the above formulas are explained in Table 1.

The monthly means are computed averaging the 12-h NCEP analyses at 1000 mb for the period 1980–88 while cloud cover monthly data have been taken from the Comprehensive Ocean–Atmosphere Data Set (COADS).

- For the salinity boundary condition we use the restoring term $\gamma_S(S^* - S)$ in the salinity equation (5), setting $K_h(\partial S/\partial z) = 0$ at the surface. This is because although we can estimate evaporation E correctly through our heat flux parameterization, knowledge of precipitation P is still limited and is characterized by large errors especially over oceanic areas. We relax the salinity to the National Oceanographic Data Center (NODC) monthly mean salinity fields S^*, with a time constant $1/\gamma_S$ of 5 days. At each time step of the model's integration the S^* field is calculated through a linear interpolation between the relevant months. This scheme implies a salt flux W_s:

$$W_s = \Delta z_1 (S^* - S)\gamma_S, \tag{10}$$

where Δz_1 is the thickness of the first model level.

Vertical velocity at the surface is taken to be zero due to the rigid-lid assumption. At the lateral walls of the basin we assume zero flux of heat and salt and $\mathbf{v}_h = 0$. At the bottom friction is set to zero $\boldsymbol{\tau}_b = 0$, the vertical velocity is $w = -\mathbf{v}_h \cdot \boldsymbol{\nabla} H$, and a zero flux condition for temperature and salinity is posed.

The model was initialized using the temperature and salinity profiles taken from the MED2 hydrological dataset (Brasseur et al. 1996). Initial fields at the model grid points and levels were produced using the Cressman (1959) objective analysis technique. The model was initially integrated for 11 yr driven by monthly mean climatological values of the atmospheric parameters $\mathbf{W}$, T_a, r_h, and C. These values were also used in Roussenov et al. (1995). The period of integration is long enough to achieve a repeating seasonal cycle over a small kinetic energy decreasing trend. At the end of this ''perpetual'' period of integration we start forcing the model with the 1980–88 monthly mean atmospheric parameters.

TABLE 2. Table of experiments.

Expt name	NCEP forcing	Initial conditions
Central	Jan 1980–Nov 1988	Perpetual year IC
Expt II	Jan 1980–Nov 1988, heat fluxes but constant wind stress	Perpetual year IC
Expt III	Jan 1980–Nov 1988, heat fluxes but zero wind stress	Perpetual year IC
Expt IV	Apr–Aug 1986	30 Mar 1981 of central expt
Expt V	Apr–Aug 1987	30 Mar 1981 of central expt
Expt VI	Apr–Aug 1981	30 Mar 1986 of central expt
Expt VII	Apr–Aug 1987	30 Mar 1986 of central expt
Expt VIII	Apr–Aug 1987	30 Mar 1984 of central expt

In Table 2 we show the series of experiments discussed in the paper. Apart from the central experiment, we performed two experiments for the 9 yr of the time series but with constant (expt II) and zero wind forcing (expt III), keeping everything else the same as in the central experiment. The constant wind stress field is computed as the climatological annual average of the 9-yr time series. Experiments IV–VIII were designed in order to study the effect of winter conditions in setting the ''memory'' of the Mediterranean Basin circulation and will be discussed in section 6.

3. Momentum and heat budgets at the surface

a. Momentum fluxes

Due to its geographic location, the Mediterranean is exposed to a general atmospheric westerly flow that subsequently interacts locally with the rich and complicated orography of the region ending up in a regionally modified atmospheric flow field (Ozsoy 1981). The most important effect is the orographic channeling of air masses into the region. A typical example of this interaction is the Mistral, which is a cold and dry wind blowing through the Rhone Valley and over the Gulf of Lions area and the Bora blowing through the Alps and the Dynaric Alps. The climatological seasonal wind stresses have been described in Roussenov et al. (1995). The most important characteristics during the winter period is the zonal character of the wind field over the entire EMED area and the northwesterly Mistral wind jet blowing over the WMED. Increased zonality, particularly in the EMED, can be partially attributed to the averaging technique used in order to produce the monthly climatology (Myers et al. 1998). However, the Hellerman and Rosenstein (1983) climatology also shows a more pronounced zonality in the winds during winter

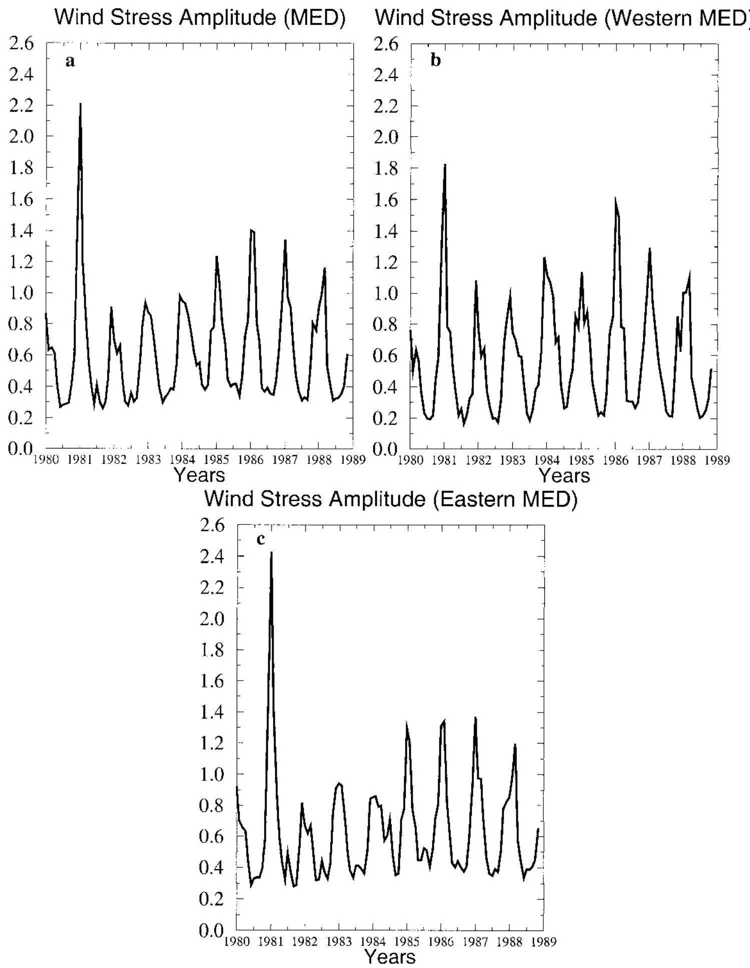

FIG. 2. (a) Surface integral of the wind stress amplitude over the Mediterranean Basin vs time (1980–88, central expt). The units are dyn cm^{-2}. (b) Surface integral of the wind stress amplitude for the WMED vs time (1980–88). (c) As in (a), (b) but for the EMED. (d) Surface integral of the wind stress curl over the Mediterranean Basin vs time (1980–88, central expt). The units are 10^{-1} dyn cm^{-3}. (e) As in Fig. 2d but for the WMED. (f) The same as in Fig. 2d but for the EMED.

than summer. The summer regime is characterized by the weakening of the Mistral wind pattern in the WMED and by the change in wind direction in the Aegean and Levantine area where northwesterly winds prevail during summer (Etesian winds).

The winter wind stress fields produce a wind curl field that is positive in the greatest part of the basin and only changes sign along the southern sector of the EMED (see Roussenov et al. 1995). During the summer period the wind stress curl becomes negative in the Ionian and the Algerian–Provencal areas. However the positive wind stress curl over the Rhodes gyre and the Aegean Sea persists throughout the year. The wind stress amplitude and curl are shown in Fig. 2. The largest anomalies are in the winters of 1981 and 1986 in the WMED and 1981 in the EMED. In Fig. 3 we show the structure of the wind stress fields for the months of January and August as typical winter and summer conditions and for 1981, 1984, 1986, and 1987. We note the intensification of the wind pattern during winters of 1981 and 1986. In 1981 the wind is blowing from the northwest in the entire basin with the exception of the Levantine area where the wind is zonal, while during 1986 it becomes zonal in the WMED and southwesterly in the EMED. Inspection of the wind patterns shows a stronger interannual variability characterizing the winter conditions as compared to the summer counterparts.

b. Heat fluxes

In Fig. 4a we show the basin-averaged total surface heat flux time series computed by the model during the 9-yr central experiment simulation. Note the very strong negative anomalies during the winters of 1981 and 1987 and the positive anomalies (net warming) during the summers of 1987 and 1988. Separate time series for the

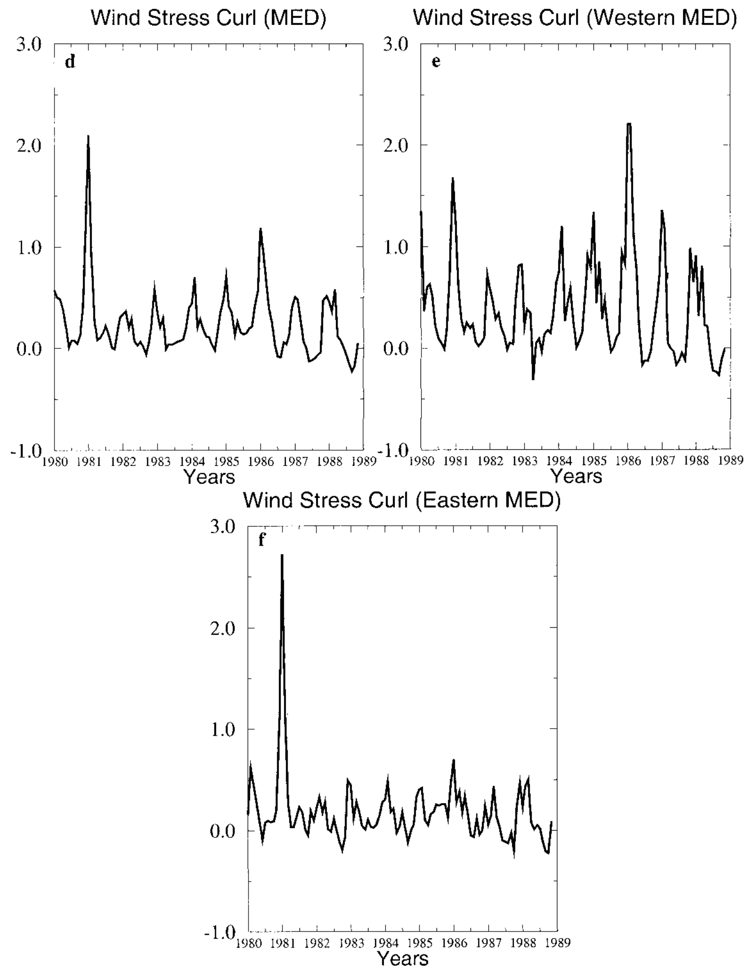

FIG. 2. (*Continued*)

WMED and EMED, shown in Figs. 4b and 4c, look very similar but we note that the 1981 negative peak is larger for the EMED while the 1987 is larger for the WMED. In Table 3 we summarize the annual surface-averaged heat flux for the whole Mediterranean Basin (SHB_1) and separately for the WMED (SHB_2) and EMED (SHB_3). Heat transports are calculated at the Gibraltar and Sicily sections for the WMED and EMED, respectively. The heat transport (in watts) through any section is defined as

$$HT_{l_1 l_2} = \rho_o C_p \int_{l_1}^{l_2} \int_{-H}^{0} (\mathbf{v}_h T + A_h \nabla^3 T)\hat{n}\, dz\, dl, \quad (11)$$

where l_1, l_2 are the extremes of the section and $\hat{n}$ is the unit vector normal to the section. Thus, $HT_1 = HT_{GIB}/S_{MED}$, $HT_3 = HT_{SIC}/S_{EMED}$, and $HT_2 = (HT_{GIB} - HT_{SIC})/S_{WMED}$ (where S_{MED}, S_{WMED}, and S_{EMED} are the surface areas of the Mediterranean, the WMED, and the EMED, respectively). Positive values of the heat transport are found at Gibraltar (HT_1) and at Sicily (HT_3), meaning that the Mediterranean imports heat from the Atlantic and the WMED exports heat into the EMED. The total (annual) heat flux for the whole basin varies between the extreme values of $+14.5$ W m^{-2} in 1987 and -4 W m^2 in 1986. It is noticeable that throughout the years of integration the heat budget of the WMED is strongly positive while the EMED can be losing or gaining heat from the surface on an annual basis. We note that the winter anomalous wind years of 1981 and 1986 are the only ones giving a net heat loss on the overall basin. This annual heat budget is clearly shifted toward a warm climate for the Mediterranean. We believe that this is the reason for the possible climate drift of the model and we think that the possible sources of errors are the inaccurate representation of coarse-grid Gibraltar processes and/or inaccuracies in knowledge of atmospheric forcing. Finally we notice that HT_1 and SHB_1 are not compensating on an annual basis. On the other hand HT_2 and SHB_2 are closer to a balance while HT_3 and SHB_3 are not even compensating in sign for some years. This means that the WMED is loosing the surface heat flux information variability more rapidly than the

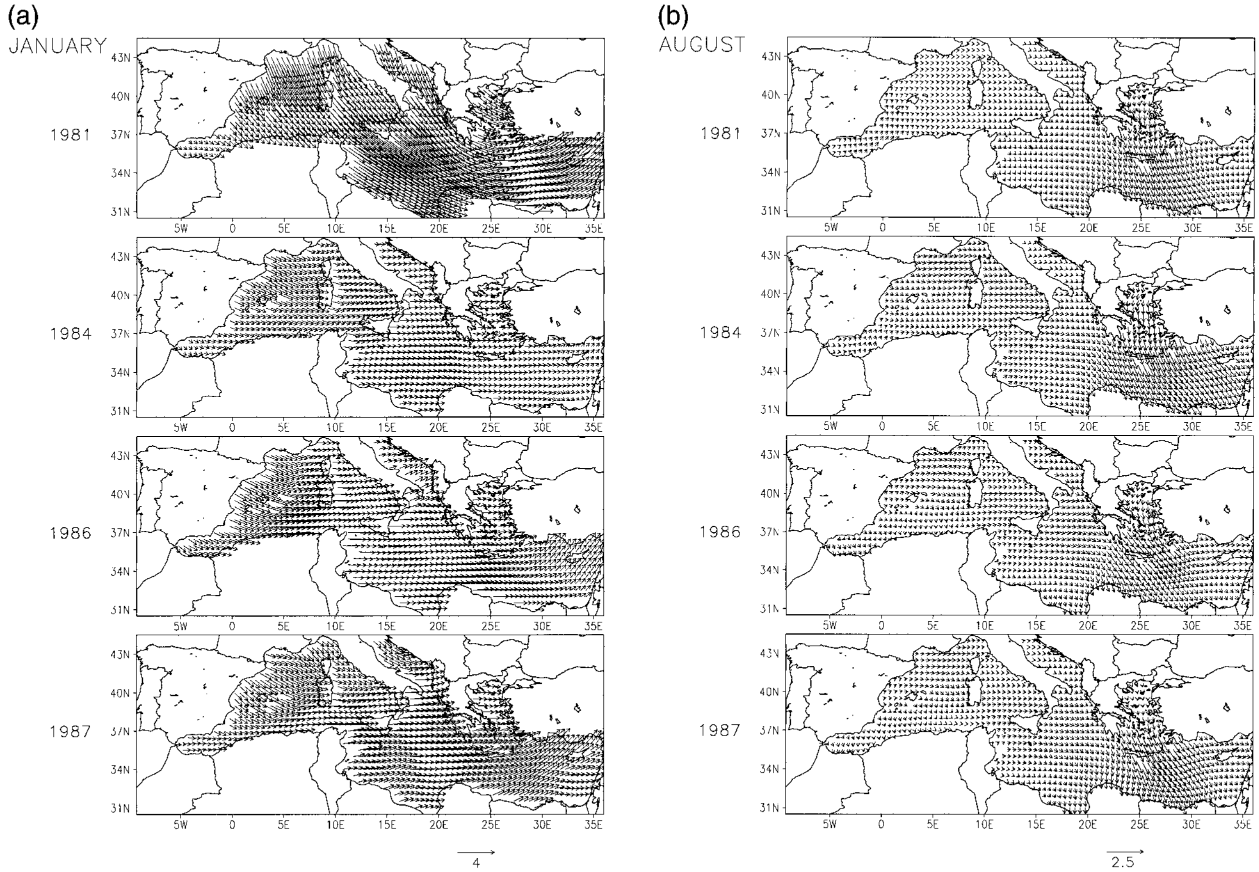

FIG. 3. Wind stress fields computed by the model for 1981, 1984, 1986, and 1987 (central expt): (a) for Jan and (b) for Aug. The units are dyn cm^{-2}.

EMED, which can store the heat flux anomalies independently from annual heat flux.

The climatological patterns of Q_T are described by Roussenov et al. (1995). Following their work, a net heat loss takes place during autumn and winter while spring and summer are characterized by a net heat gain. Local maxims of heat loss are observed in the northern Balearic, the northwestern Levantine area during the winter months (December, February), and the Adriatic area. The boundary-intensified character of the heat forcing in the Mediterranean, pointed out by Roussenov et al. (1995), is present also in the interannual fields. The southern boundary of the Mediterranean (North African coasts) is the area of minimum heat gain during summer and maximum heat loss during winter. In Figs. 5a,b we show the interannual variability of the heat fluxes for January and August of 1981, 1984, 1986, and 1987. Note the intense heat loss along the southern boundary and in particular in the Gulf of Sirte area (-420 W m^{-2}) and in the Gulf of Lions area (-320 W m^{-2}) during January 1981. January 1987 constitutes the second strongest heat loss anomaly, which lasts for two months (January and February), to the contrary of 1981, which is only for one month. The positive heat flux anomaly of summer 1987 involves highly increased heat gain mainly in the eastern Levantine area.

4. Steady-state components of the Mediterranean circulation

We start the discussion of the Mediterranean circulation by showing the basin-average kinetic energy fluctuations and the climatological dynamic height, barotropic streamfunction, and total velocity fields obtained by averaging the 9-yr time series of model fields. In the next section will show how this climatological steady-state picture of the circulation changes on the seasonal and interannual basis so our scope here is to briefly define the amplitude and structure of the general circulation to be compared with seasonal and interannual fluctuations.

The kinetic energy time series of the central experiment is shown in Fig. 6 and it is evident that the basin amplifies its circulation in response to the wind forcing anomalies of the winters of 1981 and 1986 (shown in Figs. 2 and 3a). These two winters involve the highest (cyclonic) vorticity input by the wind over the basin as shown in Fig. 2d. It is constructive at this point to at-

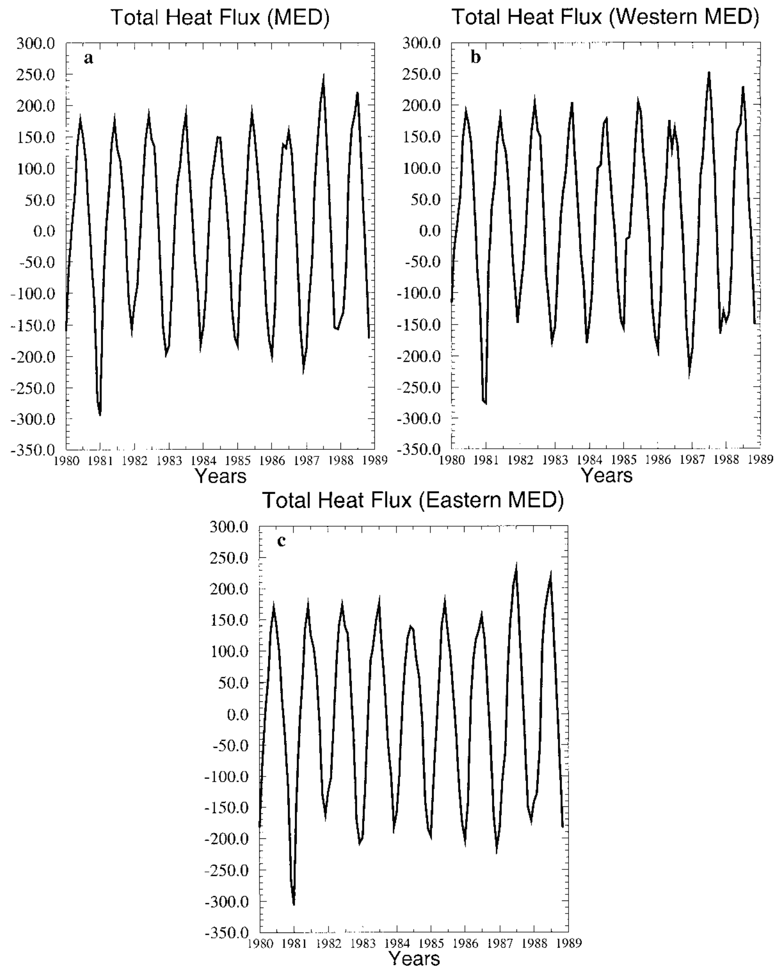

FIG. 4. (a) Surface integral of the total heat flux Q_T vs time (1980–88, central expt). The units are W m^{-2}. (b) Surface integral of the total heat flux Q_T for the WMED vs time (1980–88, central expt). (c) As in Fig. 4a but for the EMED.

tempt a separate examination of the basin-averaged kinetic energy, wind stress amplitude, and wind stress curl time series for the WMED and the EMED. These are shown in Fig. 6 for the kinetic energy and in Fig. 2 for the wind stress amplitude and curl. The wind anomaly of 1981 amplifies the circulation in the WMED only slightly, while on the other hand the EMED responds by a drastic increase in its kinetic energy content. The magnitude of the wind stress anomaly being only 30% different in the two basins (see Figs. 2b,c) cannot account for the 300% difference in the EMED kinetic energy level. We conclude and show in Part II that it is the internal dynamics of the EMED that imposes an amplifier-type character to this basin (see also section

TABLE 3. Interannual variability of annual mean surface heat budget (SHB) and transports (HT). Here, HT_1 is the net heat transport at the Gibraltar Strait; HT_2 is the net heat transport for the WMED; and HT_3 is the net heat transport at the Sicily Strait as defined in section 3.2.

Year	MED (W m^{-2}) SHB_1	MED (W m^{-2}) HT_1	WMED (W m^{-2}) SHB_2	WMED (W m^{-2}) HT_2	EMED (W m^{-2}) SHB_3	EMED (W m^{-2}) HT_3
1980	0.076	1.380	12.894	−8.608	−6.804	6.716
1981	−1.591	1.425	14.012	−9.429	−9.960	7.224
1982	11.234	1.227	24.054	−13.229	4.359	8.948
1983	7.175	1.107	16.356	−9.177	2.257	6.600
1984	7.681	1.020	18.408	−11.244	1.926	7.571
1985	5.940	0.901	23.174	−11.318	−3.306	7.428
1986	−3.946	0.873	6.205	−7.744	−9.396	5.476
1987	14.553	1.144	23.037	−10.416	9.999	7.379

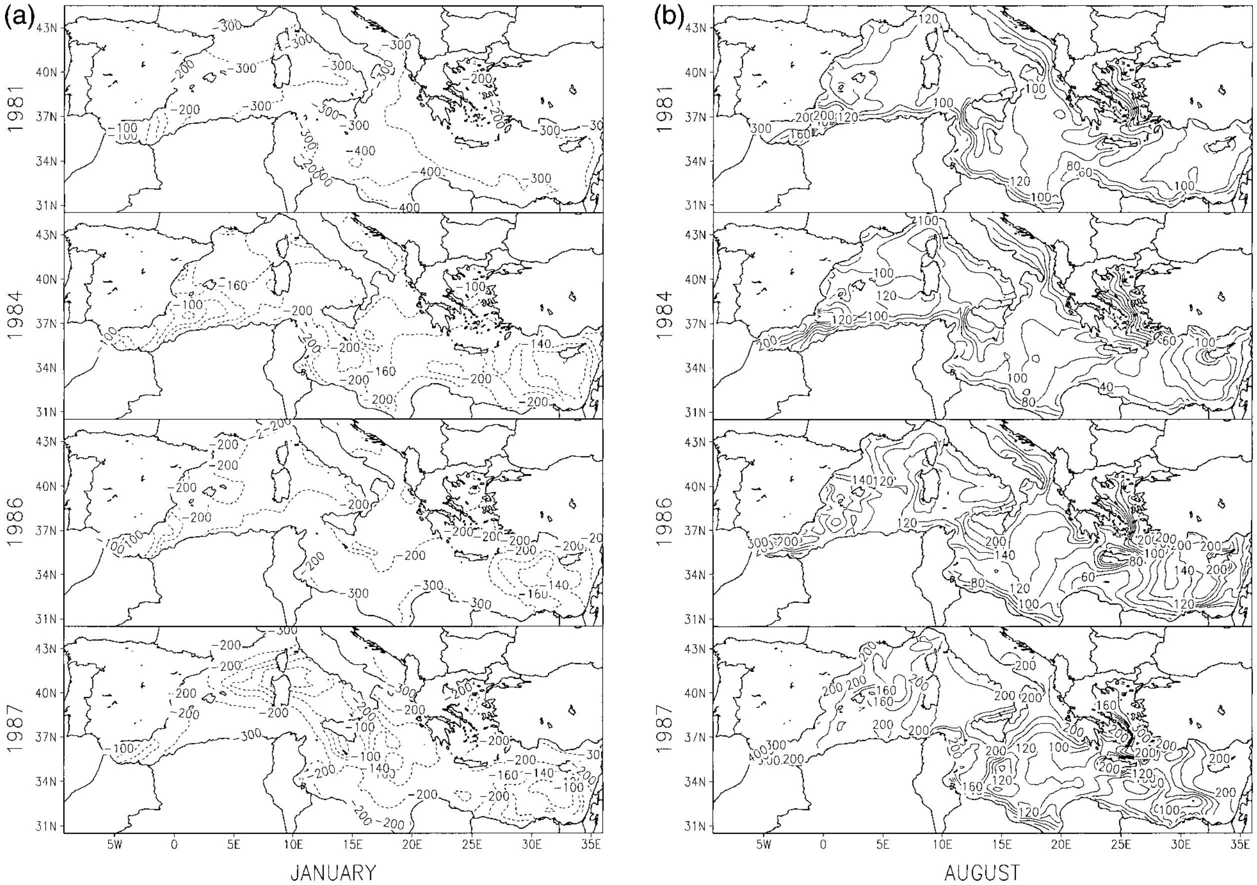

FIG. 5. Total heat flux fields for (a) Jan and (b) for Aug of 1981, 1984, 1986, and 1987 (central expt). The units are W m^{-2} (contour interval 20 W m^{-2}).

6). The same kind of behavior is observed during 1986 where although the wind stress anomaly is higher for the WMED, the EMED circulation kinetic energy is amplified in a comparable way. Thus the interannual variability of the wind stress forcing during these 9 yr corresponds to two anomalous wind stress amplitude and curl anomalies, the first in the EMED in 1981 and the second in the WMED in 1986. This produces interannual variability in the kinetic energy content of the general circulation. We note also that the basin-average kinetic energy is amplified for wind stress curl anomalies more than wind amplitude changes. This is the difference between the winters of 1986 and 1987, which give radically different ocean responses in terms of kinetic energy of the general circulation while the amplitude of the winter wind stress anomaly is the same.

In Figs. 7a–c we show the steady-state component of the dynamic height fields at 30, 100, and 300 m calculated with a reference level of 450 m in order not to exclude the relatively shallow areas of the basin. In Fig. 7d we show the barotropic streamfunction ψ, defined by the relationship

$$\overline{\mathbf{v}}_h = \frac{\hat{k} \times \nabla\psi}{H(x, y)}, \tag{12}$$

where $H(x, y)$ is the bottom relief, ψ is the streamfunction, and $\overline{\mathbf{v}}_h$ is the depth-integrated velocity, that is, $\overline{\mathbf{v}}_h = (1/H) \int_{-H}^{0} \mathbf{v}_h \, dz$.

In the WMED we see at the surface a well-developed Algerian current, which east of Majorca bifurcates with one branch going to the north and recirculating into the Lions gyre. The other branch continues eastward along the African coast exhibiting a large meandering into the central Balearic Basin. The Lions gyre displays a well-defined cyclonic structure in its approximate climatological geographical location. The Tyrrhenian circulation itself is cyclonic, sucking Atlantic waters near the western tip of Sicily. To the north of this basin through the Corsican Channel waters move northward into the Ligurian Sea feeding the boundary current flowing along the French coast (Ligurian–Provencal current).

At 300 m we observe the flow of LIW entering into the WMED from the Sicily Strait and subsequently flowing into the Tyrrhenian basin following a well-defined cyclonic path. After the southern tip of Sardinia it splits into two branches, the strongest going northward joining the Lions gyre and the other westward into the Alboran Sea and subsequently to the Atlantic Ocean through the Gibraltar Strait. This is in agreement with the clima-

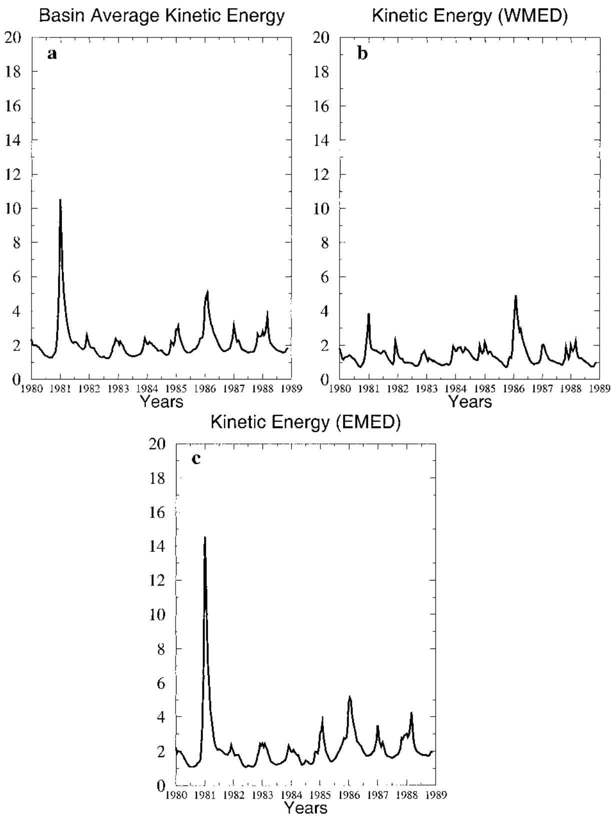

FIG. 6. (a) Volume-integrated kinetic energy (in ergs cm^{-3}) of the Mediterranean Basin vs time for 9 yr (1980–88) of interannual integration (central expt). (b) As in Fig. 6a but for the western basin. (c) As in Fig. 6b but for the eastern basin.

tological picture presented by Wust (1961) and Ovchinnikov (1966). The westward branch of the LIW path is hereafter called the Algerian undercurrent and it will be discussed in detail later.

The deep flow at 700 m is shown in Fig. 7g and it is characterized by smaller spatial scale gyres. A series of cyclonic–anticyclonic features are present along the African coast while the Lions gyre appears still cyclonic but reduced in size. The same happens with the Tyrrhenian cyclone, which is confined to the western part of the basin while a hint of anticyclonic circulation is present in the eastern part of it.

In the EMED the surface steady-state circulation consists of the Ionian–Atlantic stream that, after leaving the Sicilian plateau, turns to the southeast and flows eastward to become the Mid-Mediterranean jet, which then branches to the north at the western and eastern sides of Cyprus feeding the Asia Minor current (Robinson et al. 1991). The Western Ionian cyclone (Roussenov et al. 1995) is well developed at intermediate depths where it is fed by waters flowing westward from the Aegean western strait.

The Rhodes gyre is a well-developed feature throughout the water column and it is positioned southeast of Crete. The signature of the Mersa–Matruh anticyclonic gyre becomes evident at 300 m where we also see an anticyclonic pattern south of Cyprus corresponding probably to the Shikmona gyre. At 300 m we see that the LIW current to the WMED is fed by two boundary currents, one flowing southward along the Italian coast and the other flowing westwards along the Libyan coast. Both boundary currents are fed by waters outflowing from the Levantine area.

The deep flow (700 m) consists of two anticyclones (Sirte and Mersa–Matruh gyres) in the southernmost part of the basin and three cyclonic centers: the Rhodes, the western Crete, and the western Ionian gyres. At this depth the central Ionian is occupied by an anticyclonic pattern encompassing the Sirte anticyclone. The western Ionian Basin is occupied by the Western Ionian cyclone, which borders with a southward boundary current along the Italian coast.

5. Upper-thermocline interannual variability

a. Surface flow field variability

The discussion on the flow fields seasonal/interannual variability starts by investigating the main circulation patterns and the changes they undergo at the depth of 30 m, which is approximately located at the bottom of the surface Ekman layer and within the AW layer. In this section we refer to Fig. 8 where we show the total velocity fields for the months of February and August of 1981, 1984, 1986, and 1987 from the model central experiment of Table 2.

1) ALGERIAN CURRENT

The Algerian current variability exhibits several interesting aspects having implications on the circulation of the Western Basin. During summer the Algerian current seems to be more unstable probably due to the increased inflow from the Straits of Gibraltar in this season, as shown also by Roussenov et al. (1995). Its meandering activity varies from year to year and in August 1986 we notice an almost complete cutoff of a large anticyclone in the Balearic Basin. During the summer of 1987 the current, after exiting the Alboran Sea, bifurcates and its northern branch flows anticyclonically around the Balearic Islands. As pointed out by Herbaut et al. (1996, 1997) the Algerian current is mainly driven by the Gibraltar inflow and it undergoes baroclinic instability meander growth. However, we see here differences from year to year that cannot be related entirely to changes in strait inflow, which are altogether small (see Fig. 14). Our conclusion is that local atmospheric forcing over the Balearic Basin can cause changes in the strength, direction, vertical shear of the current, and ring cutoff events but we cannot be very conclusive since the model is too coarse to resolve the meander and ring growth processes. Later in the paper, we discuss changes in the Algerian deep current, which we show are related to changes in atmospheric forcing.

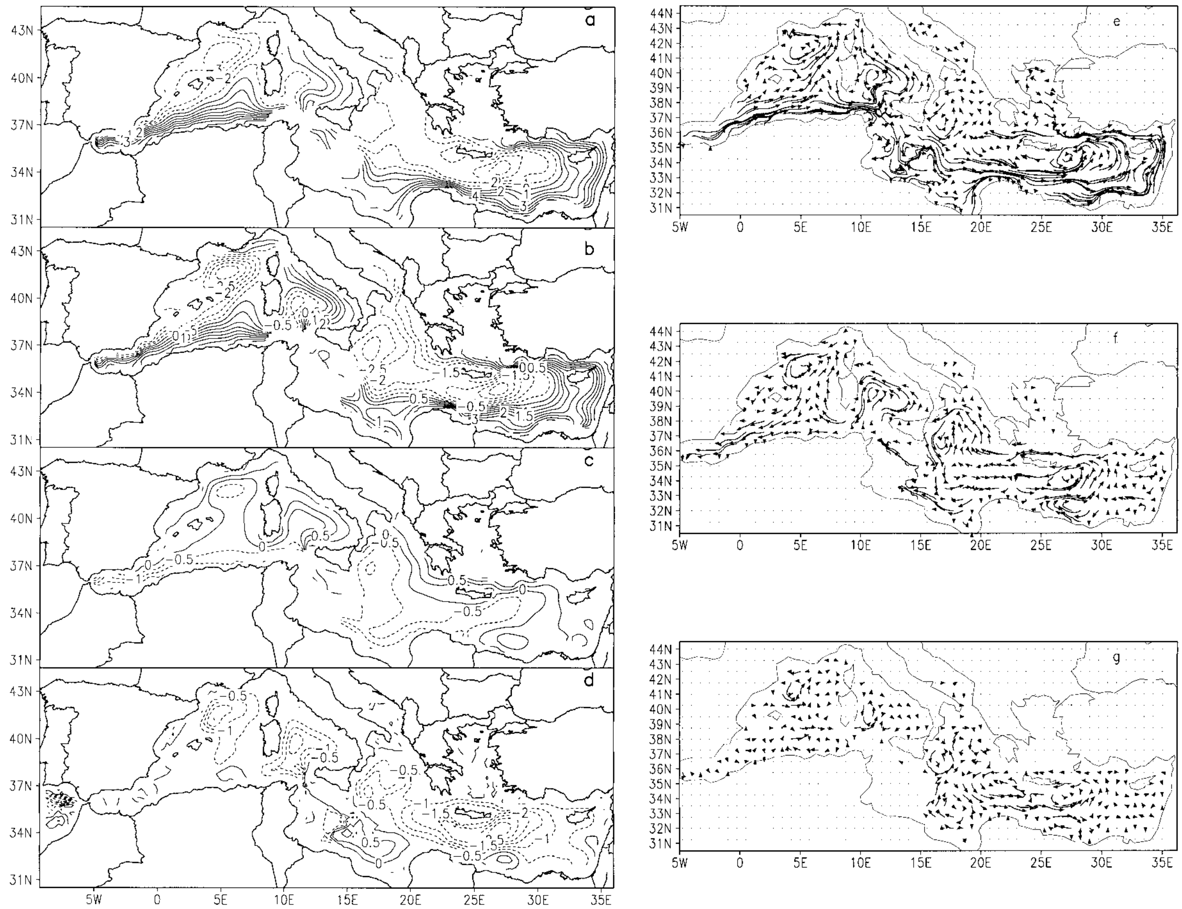

FIG. 7. Steady-state components of the Mediterranean circulation (central expt). Dynamic height (cm) calculated with a reference level at 450 m at (a) 30 m (c.i. 1 cm), (b) 100 m (c.i. 0.5 cm), and (c) 300 m (c.i. 0.5 cm); (d) barotropic streamfunction [1Sverdrup (Sv) = $10^6 m^3 s^{-1}$] field (c.i. 0.5 Sv), (e) 90-day particle trajectories at 30 m, (f) 180-day particle trajectories at 300 m, and (g) 270-day particle trajectories at 700 m.

2) LIONS GYRE

The Lions gyre is reproduced by the model as a persistent feature of the WMED circulation appearing to be more spatially extended during the winter period and more restricted during summer. Its location remains more or less the same although it undergoes seasonal and interannual shape and location changes. Here the winter interannual variability of the gyre surface signature and strength is mainly due to the wind anomalies. In summer the wind forcing is much weaker (Fig. 2b) and therefore heat anomalies are responsible for the interannual variability of the surface flow field.

3) TYRRHENIAN SEA

The winter Tyrrhenian circulation consists of a well-developed cyclone occupying the whole basin area. Part of the Algerian current carrying AW waters eastward becomes entrained in the cyclonic circulation near the western tip of Sicily. The winter interannual variability can be related to both wind and heat flux anomalies but the wind anomalies seem to be more important. Differences between the central experiment and experiments II and III (not shown) demonstrate that wind is a major driving force in this basin. In the case of 1981 and 1986 the amplified cyclonic circulation (Fig. 8) was absent when winds were not considered. The winter and summer variabilities mainly show up as an eastern boundary current (winter) and northward central basin current (summer). The winter to summer variability and especially the summer reversal of the eastern Tyrrhenian circulation agree with the results of Pinardi and Navarra (1993), Zavatarelli and Mellor (1995), and Roussenov et al. (1995) and the climatological seasonal variability of the circulation from historical data (Tziperman and Malanotte-Rizzoli 1991). In experiments II and III, which used constant and zero wind stress but interannual heat fluxes, the summer reversal does not occur. The recent work of Herbaut et al. (1997), which uses a high horizontal resolution model of the western Mediterranean, confirms the importance of wind forcing in the structure of the circulation of the Tyrrhenian Sea and of the whole WMED, in general.

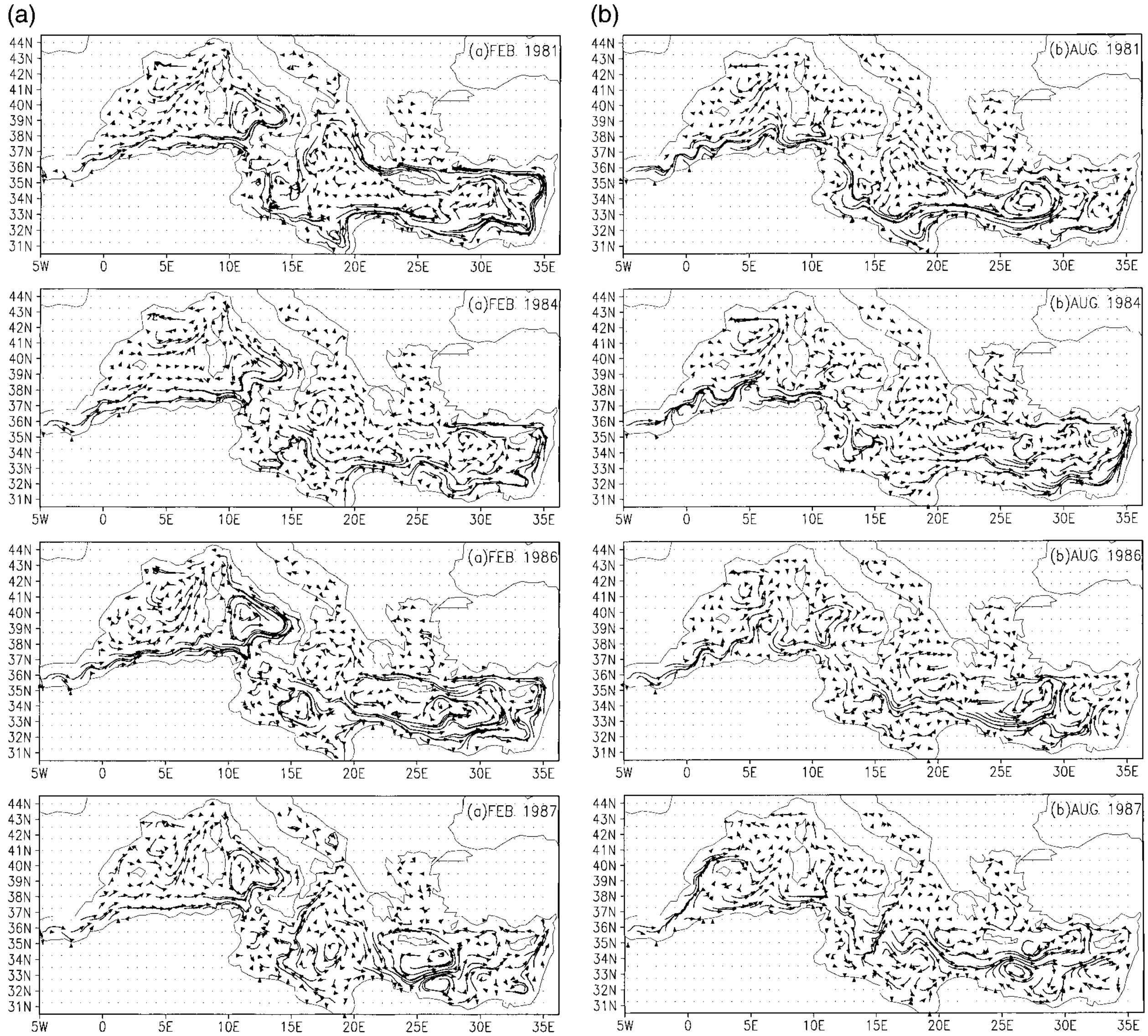

FIG. 8. The 30-day particle trajectories fields at 30 m for Feb and Aug 1981, 1984, 1986, and 1987 (central expt).

4) IONIAN–ATLANTIC STREAM

The Ionian–Atlantic stream flows in general to the southeast after leaving the Sicily shelf plateau bordering the Sirte anticyclone and meandering at about 35°N. It is only after the eastern tip of Libya that the current hugs the African coast again. In cases where the Sirte anticyclone is absent, like during summer 1981, the current shoots to the coast right after exiting the Sicilian plateau. In summer of 1987 the current experiences a bifurcation after the eastern tip of Sicily with a southern branch bordering the Sirte anticyclone and a northern branch flowing the Italian coast. Bifurcations and meandering of the stream occur also in the summer of 1984. The northward branching of the stream in the summer of 1987 is confirmed by observations, as shown in section 9.

5) WESTERN IONIAN CYCLONE

The western Ionian cyclone is a recurrent feature of the Ionian circulation. During the summer period it appears to be more restricted to the west due to the development of an anticyclonic pattern in the eastern Ionian area. In the winters of 1982 (not shown here) and 1987 the central Ionian area is occupied by an extended anticyclonic pattern and the western cyclone dies out.

6) MID-MEDITERRANEAN JET

The mid-Mediterranean jet (MMJ), which is the continuation of the Ionian–Atlantic stream in the Levantine Basin, is evident at the border between the Rhodes and Mersa–Matruh gyres. Its position is controlled by the relative strength, shape, and location of those two gyres.

During wintertime the MMJ flows along the African coast because of the extension and intensification of the Rhodes gyre, which occupies the central Levantine area. Exceptions to this are the winters of 1984 and especially of 1987 where a relatively strong Mersa–Matruh forces the MMJ to deviate from the coast and flow midway between Crete and the African coast. The MMJ bifurcates southwest of Cyprus with one branch flowing cyclonically around Cyprus and feeding the Asia Minor current. However during the summer of 1987 there is a double bifurcation east of Cyprus with the southern branch feeding the Shikmona anticyclone.

7) LEVANTINE BASIN

The Rhodes gyre is a well-defined feature during all seasons but is clearly more intense during wintertime undergoing interannual variations in strength and shape. During 1981 and 1986 we see a strong intensification of the gyre and a displacement of its center to the southeast of Crete. The Rhodes gyre center displacement from year to year is probably a feature connected with the uncertainty in the atmospheric forcing and missing topographic effects in our model. We argue that interannual variability may be more realistic in the shape and strength of the gyre and not in its center location. The Mersa–Matruh anticyclone, which is mainly a subsurface feature, is found to be well developed during the summer period in general. However we have already seen cases like those of 1984 and 1987 where the gyre persists also during the winter period. The Asia Minor current appears to be a permanent feature of the Levantine circulation, exhibiting seasonal/interannual changes in its strength. It contributes to the northern intensified border of the Rhodes gyre and it is fed by the two branches (west and east of Cyprus) of the MMJ. During the winter period, the current intensifies but relaxes during summer. During the winters of 1981 and 1986 it is highly amplified due to the wind forcing action. The strong interannual variability observed in the Levantine area can be attributed to the action of the wind (mainly) and the thermohaline forcing as we can conclude by comparing the results of the central with the constant (expt II) and zero wind (expt III) experiments.

The Shikmona gyre is present at the surface only starting from 1984 and it reaches maximum amplitude in summer 1987. In the subsurface the gyre is more visible and it will be described in the next section.

b. Intermediate-depth flow field variability

We present here the flow fields at 300 m for February and August of 1981, 1984, 1986, and 1987 (Fig. 9). This level lies at the center of the climatological LIW layer in the model. LIW is formed in our model within the Rhodes gyre area, generally known as the prominent LIW formation area (Lascaratos et al. 1993). The *T–S* characteristics of our LIW water are $T \sim 17.5°$C and $S \sim 38.95$ psu, which give a $\sigma_i \sim 28.3$. This density value is out of the range of values described by Lascaratos et al. (1993) due to $\sim$1.5°C higher temperature values in our model than in the observations. The water is formed usually in February and the mixed layer depths range between 100 and 300 m depending on the strength of the winter cooling. After its formation, LIW is advected out of the Rhodes gyre and it is present in most areas of the basin throughout the year. We will not describe in detail the spreading mechanisms of LIW since it is believed that eddies play an important role in this process (Haines and Wu 1995; Wu and Haines 1996). Again we focus our discussion on the main features of the horizontal circulation and its variability. Since LIW is formed in the EMED we start this time by describing the EMED first. At this depth a system of subbasin-scale gyres that are either permanent or recurrent on a seasonal or interannual basis is evident at first inspection.

1) EASTERN LEVANTINE BASIN

The Rhodes and the Mersa–Matruh gyres are characterized by strong interannual fluctuations in strength and shape, and therefore it is rather difficult to identify their seasonal characteristics. However the Mersa–Matruh anticyclone tends to appear as a well-developed structure during summer periods although we see cases where it develops during winter periods as well (winters of 1984 and 1987). On the other hand the Rhodes gyre usually appears to be elongated during the summer period having a SW–NE orientation but it is evident throughout the year. In cases where the Mersa–Matruh gyre weakens and shrinks (as during the winter period) the Rhodes gyre expands and occupies a considerable portion of the central Levantine area. The variability of both gyres is controlled by the action of wind and thermohaline forcing as we can deduce from the comparison of the central experiment with experiment II. However the wind is the most important forcing again. The Shikmona anticyclone is present south of Cyprus every summer but with significant differences in strength and location while during winter it is sometimes totally missing.

2) IONIAN BASIN

In the Ionian Basin there is an eastern boundary current carrying LIW to the north fed by waters flowing westward north and south of Crete. It is confined along the Greek coasts during the winter period and shifts southwest during summer due to the development of an anticyclone in the northeastern Ionian area where the Pelops gyre is reported to be by Robinson et al. (1991). This anticyclone is not well defined throughout the years of integration and for example during summer 1984 is totally absent. A branch of this eastern boundary current

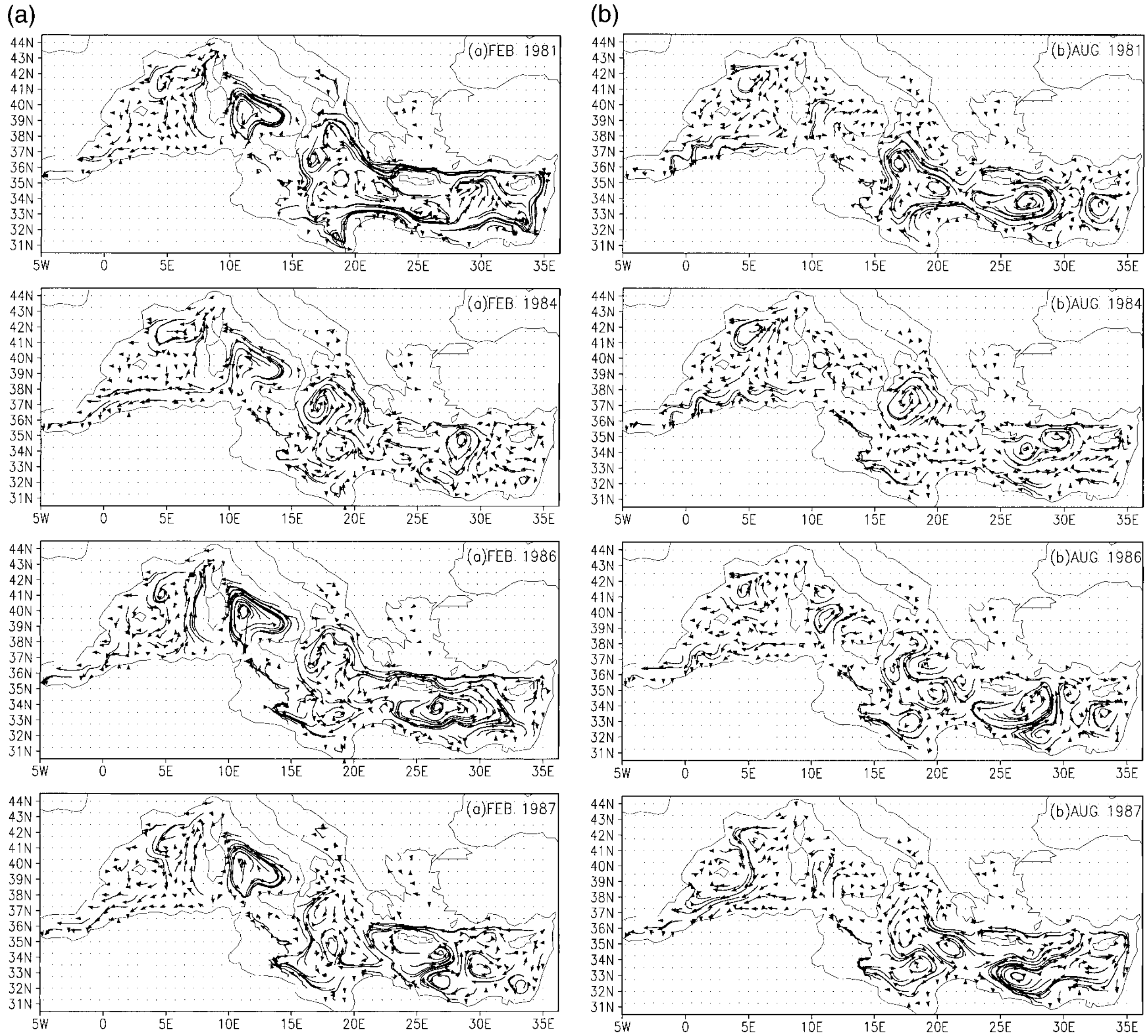

FIG. 9. The 90-day particle trajectories fields at 300 m for Feb and Aug 1981, 1984, 1986, and 1987 (central expt).

turns westward in the central-north Ionian merging with the border of the western Ionian cyclone. During the winter and summer of 1981 and the winter of 1986 this eastern current appears to be strongly intensified. The westward flow going through the Sicily Strait is partially fed by the western Ionian cyclone and by a southern boundary current flowing along the African coast. The western Ionian cyclone weakens dramatically during the winter of 1987 where we observe instead an anticyclone in the western-central Ionian area. In this case the outflow of LIW from the EMED consists mainly of the southern boundary current.

3) WMED

In the WMED the seasonal changes constitute the main signal of variability at 300 m. During winter months, the LIW outflow from the Sicily Strait enters immediately the Tyrrhenian Basin at the western tip of Sicily. Subsequently the LIW mean current flows along the Italian coast, turning cyclonically in the Tyrrhenian, and exits at the southern tip of Sardinia (Sardinia Channel). The most prominent interannual event in the Tyrrhenian takes place during the winter of 1986 and involves the amplification of the whole cyclonic circulation of this basin. During the summer period the cyclonic circulation is confined to the southwestern part of this basin while the eastern part of it is characterized by the presence of an anticyclonic pattern.

In the winter period, the LIW branch turns to the north around Sardinia and contributes to the cyclonic circulation in the north Balearic Basin. It is this LIW northward boundary current that contributes to the rate of deep water formation in the Gulf of Lions (Wu and

Haines 1996). However during the winter of 1984 the path of LIW south of Sardinia alters and we observe a bifurcation with one branch flowing directly along the North African coast reaching the Alboran Sea. This is the Algerian undercurrent already mentioned in section 4. During summer the situation changes completely. The LIW after exiting the Tyrrhenian Sea progresses directly to the Alboran Sea flowing along the North African coast. The branch that during winter months goes to the north is now very weak while the Algerian undercurrent is well developed.

The interannual variability of the Algerian undercurrent is highly dependent on the curl of the wind forcing over the WMED (Fig. 2e). During the winter period the strong wind forcing, which involves a highly positive curl, seems to inhibit the development of the undercurrent and thus the main LIW is to the north along the Sardinia continental margin. However whenever the wind relaxes, like during the winter of 1984, we see the appearance of a well-formed Algerian undercurrent. The change of the wind curl (weakening and/or change of polarity) during summer is a favorable condition for the development of the undercurrent that drives LIW directly toward Gibraltar. In Fig. 10 we show the average eastward and westward mean volume transport time series from the surface down to 500 m calculated as an average within the area 3°–6.6°E and from the African coast to 37.7°N (see Fig. 13) for the central and constant winds experiment (II). In experiment II we observe the existence of the Algerian undercurrent throughout the years of integration. However this is not the case for the central experiment where the Algerian undercurrent is clearly anticorrelated with the surface Algerian current and its transport reaches maximum amplitude during summer months due to the wind forcing action. In cases where the eastward flow is intensified by the wind action (like during the winters of 1980, 1981, 1986, and 1988), the undercurrent almost vanishes. We have to mention that our results are in partial disagreement with Millot (1994). He in fact shows that from June 1986 until March 1987 there is no Algerian undercurrent at 300 m at some current meter locations along the Algerian coastlines. In our case the weakening of the Algeran undercurrent happens only in winter 1986 (see Fig. 10). However it is also evident that from January 1986 up to 1988 we reach the minimum values of Algerian undercurrent transport. Some words of cautions should be said about our results since the coarse horizontal and vertical resolution may not allow the resolution of topographic effects on the Algerian undercurrent.

We would like here to speculate about the mechanisms responsible for the appearance and weakening of the Algerian undercurrent. We believe this phenomenon can be understood in terms of relative energy contained in the barotropic and first baroclinic mode components of the Algerian current. Considering a simple two-layer model of the Algerian current with the upper layer representing the AW and the lower layer the LIW water masses, the first baroclinic mode of this system would imply an Algerian upper-layer eastward current and a lower-layer Algerian undercurrent flowing westward. However if a barotropic component is excited by the wind forcing, this could put the lower layer at rest. This situation is likely to occur during winter where the barotropic mode is intensified and this could be the reason why the undercurrent is not produced in periods of strong wind forcing. On the other hand the Algerian current could be more baroclinic as happened in 1984 where the wind forcing is extremely weak.

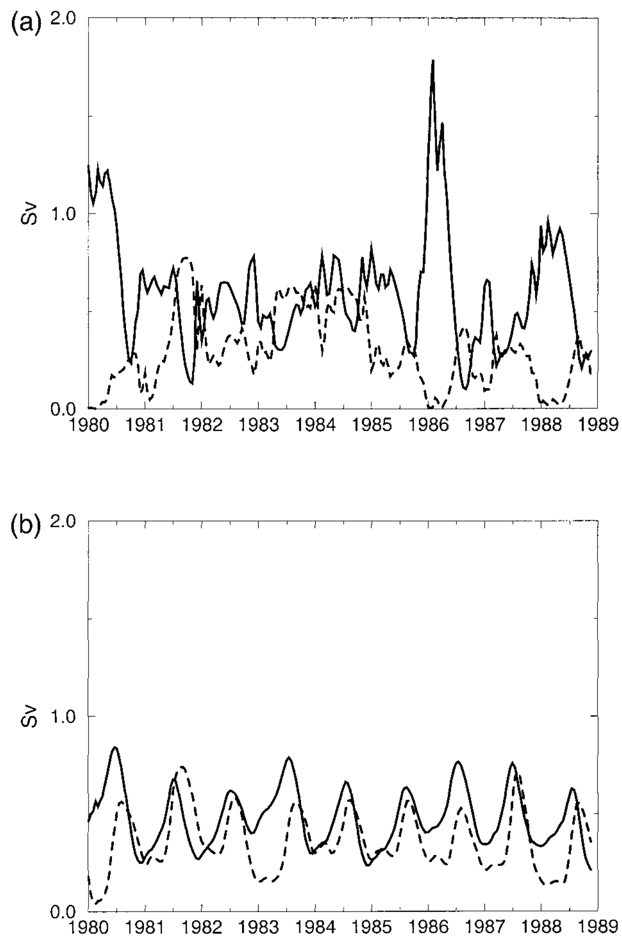

FIG. 10. Time series of mean eastward (continuous line) and westward transport (dashed line) along the Algerian coasts for (a) central expt and (b) expt II. Units are Sv.

Coming back to the description of Fig. 9, it is evident that the Lions gyre is well defined and positioned throughout the year but during the winter period it appears to be more spatially extended. The gyre is partially fed by the westward Ligurian–Provencal current, which hugs the French continental margins. The current can be intensified in different years as happens during winter 1986. North of Minorca the Ligurian–Provencal current splits into two branches, one turning eastward and the other continuing in the Catalan Sea. The branch that

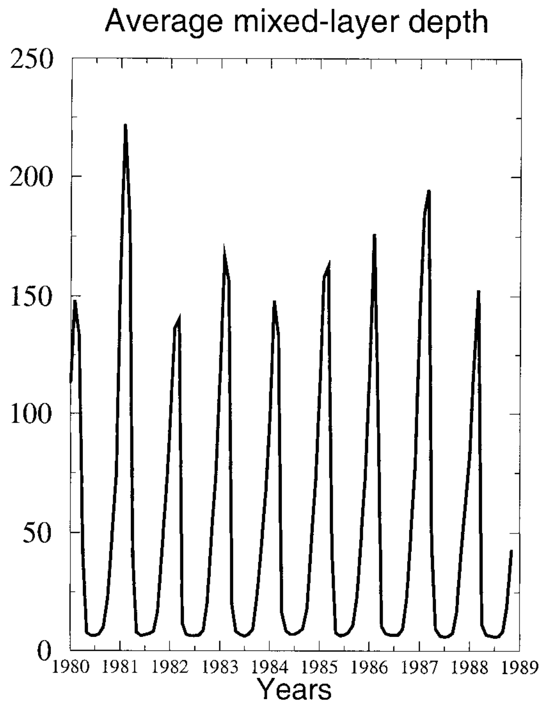

FIG. 11. Basin-averaged mixed layer depth (m) time series for the period Jan 1980–Nov 1988 (central expt).

continues to flow along the Spanish continental shelf either weakens or is not present during the summer period. Finally, south of Ibiza the two branches merge to enter the Alboran Sea.

6. On the seasonal memory of the Mediterranean Basin

We try now to elucidate the dynamical mechanisms associated with the interannual variability of the upper-thermocline currents described before. We hypothesize that the storage of information or ''memory'' of the circulation is connected to the subduction of waters occurring after winter mixed layer deepening. Thus it is plausible that rather severe winters can strongly influence the memory of the system by favoring the transformation of large amounts of surface waters into the main thermocline. The question that naturally arises is to what extent this information influences the circulation of the upcoming summer period and also what is the effect of mild winters in shaping the summer circulation. In the Mediterranean, the winter mixed layer reaches its maximum depth during February while by the middle of March it already starts to shallow. In Fig. 11 we show the time series of the surface integrated mixed layer depth. Years 1981, 1986 and 1987 involve deep winter mixed layers, which enables a drastic transfer of water masses at depths influencing the response of the basin in later months. On the other hand the winters of 1982 and 1984 involve a shallow average mixed layer over the basin due to their mild character. The mixed layer depth explains also why the interannual variability is stronger than the seasonal cycle in the EMED while the seasonal cycle is more important in the WMED. The large mixed layer depth of 1981 is in fact all concentrated in the EMED, in particular over all the Ionian Basin, while in the WMED the mixed layer never reaches great depths except for the Gulf of Lions deep waters formation area. Thus, during anomalous heat flux and wind curl winters, information is stored more efficiently in the EMED than the WMED due to the different extension of the deep mixed layer areas in the two subbasins.

In order to quantify the influence of the winter conditions on the basin circulation we decided to restart the model from the end of March 1981 for the central experiment and integrate for six more months using April–August 1986 external forcing in the first case (expt IV; Table 2) and April–August 1987 in the second one (expt V; Table 2). We wish to examine what is the circulation response of the basin during August after the application of the modified spring–summer external forcing. In Figs. 12a and 12b we show the average August total velocity fields at 30- and 300-m depth for experiments IV and V, respectively. If the fields of Figs. 12a,b are compared with the standard August 1981, 1986, and 1987 total velocity fields shown in Figs. 8 and 9 the following becomes evident.

- The flow field characteristics in the central part (between 5.8° and 32°E) of the basin at both depths are similar between experiments IV, V, and the standard August 1981 case.
- In the marginal areas of the basin (west of 5.8°E and east of 32°E) the flow field resembles the standard August 1986 and 1987 patterns and thus in these areas the external spring–summer forcing plays a crucial role in defining the circulation characteristics. To consolidate our results we performed experiments VI and VII (see Table 2), which restart from the end of March 1986 conditions and use spring–summer forcings of 1981 and 1987, respectively (not shown). Qualitatively the results are the same as for experiments IV and V. Inspection of the depth of the mixed layer for February 1981 and 1986 shows that local maxima of mixed layer depth are achieved in the Ionian and Tyrrhenian Basins while in the marginal areas of the Mediterranean the winter mixed layer remains comparatively shallow (especially west of 5.8°E) due to the milder winter wind forcing and the stronger warming during summer with respect to the central part of the basin. We argue that in areas where the winter mixed layer is deep the winter conditions can ''set'' the memory of the system modifying the circulation pattern and strength. Mild winters that involve a rather shallow mixed layer over the basin cannot strongly affect the summer circulation. In the case of experiment VIII where we restart the model from the end of March

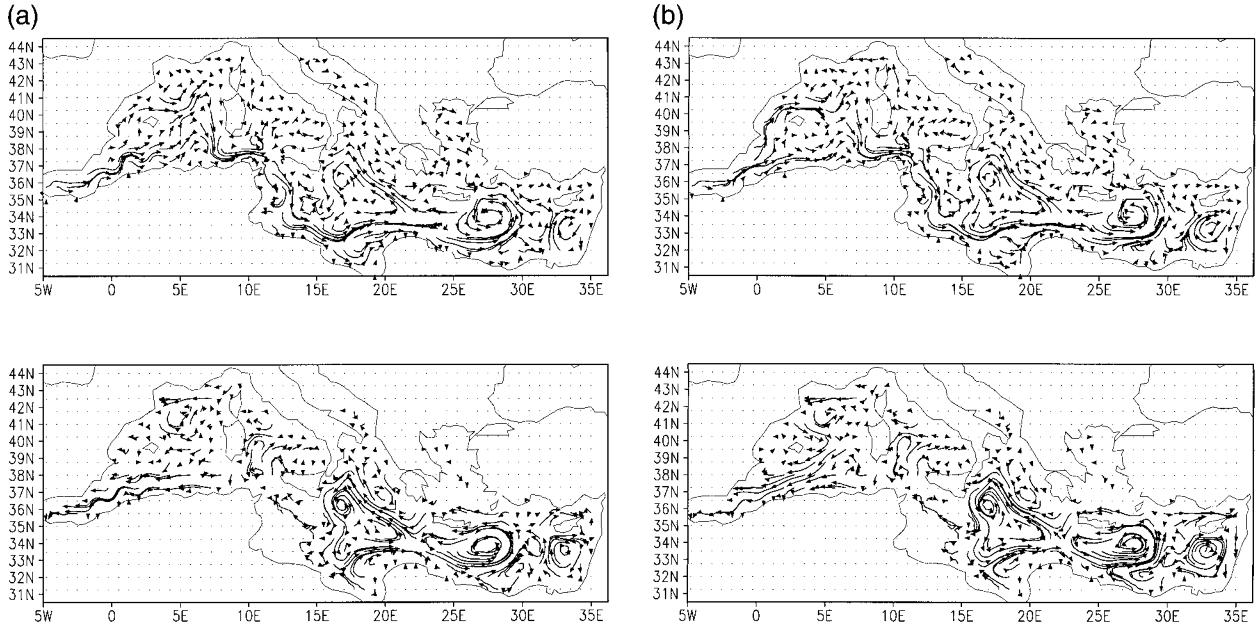

FIG. 12. (a) The 30-day particle trajectories fields at 30- (upper panel) and 90-day particle trajectories fields at 300 m (lower panel) for Aug (expt IV) and (b) as in Fig. 12a but for expt V.

1984 (a normal winter) and we integrate forward up to August using spring–summer 1987 external forcing, the summer response of the central part of the basin (not shown) is a mixture of standard August 1984 and 1987 circulation while in the marginal areas of the basin the circulation is very close to August 1987 conditions. Since the strongest interannual variability is locked to the winter months and the largest interannual forcing variability is in winter, we believe that the system memory is determined by the anomalous winters. The latter can in turn influence the following summer, shifting the occurrence of the seasonal cycle.

7. Mass and heat transport through Mediterranean sections

The Mediterranean has many straits and channels that connect different portions of the basin. They could be ideal places for monitoring the interannual fluctuations so it is important to look at the model simulation in these areas.

In the past years work has been devoted to the study of the Straits of Gibraltar role in controlling the Mediterranean circulation and climate but the lack of direct current measurements still remains a problem in assessing the various theories proposed. Lacombe and Richez (1982) gave an annual value for the AW inflow being close to 1.26 Sverdrups [1 Sverdrup (Sv) $\equiv 10^6$ m^3 s^{-1}; 1.15 Sv for the outflow] based on direct measurements. Bethoux (1979) using principles of mass, heat and potential energy conservation for the Mediterranean estimates an inflow of 1.7 Sv while Bryden and Kinder (1990) result in an inflow of 0.92 Sv (0.88 Sv for the outflow). Furthermore there is still an unresolved issue concerning the variability, either seasonal or interannual, of this transport. Bormans et al. (1986) based on historical data and hydraulic control theory conclude that the AW inflow varies seasonally with a maximum reached during spring and a minimum during fall period. At the Sicily Strait, Manzella and La Violette (1990) indicate a maximum LIW transport during December–January and a minimum during the summer period with the maximum winter value (3.2 Sv) being almost double the summer one. The same authors argue that there is a 3-month phase shift between Gibraltar (leading) and Sicily transports. Bethoux (1979) estimates a transport value of 1.2 Sv at Sicily, following the same theoretical scheme used for Gibraltar.

Layer volume transports at the Gibraltar and Sicily Strait from the central experiment are calculated according to the formula

$$\text{total layer transport} = \int_{l_1}^{l_2} \int_{-H}^{z_o} \mathbf{v}_h \cdot \hat{n}\, dz\, dl, \quad (13)$$

where l_1, l_2 are the extremes of the section, $\hat{n}$ is the unit vector normal to the section, and z_0 is the depth at which the velocity $\mathbf{v}_h\hat{n}$, perpendicular to the section, changes sign. The exact positions of the sections are shown at Fig. 13. Due to the rigid-lid assumption, the net volume transport across the Gibraltar and Sicily sections (corresponding to $z_0 = 0$) has to be zero at each time step of the model integration. This means that at Sicily the inflow from (also called AW transport) and the outflow to the WMED (also called LIW transport) have to be

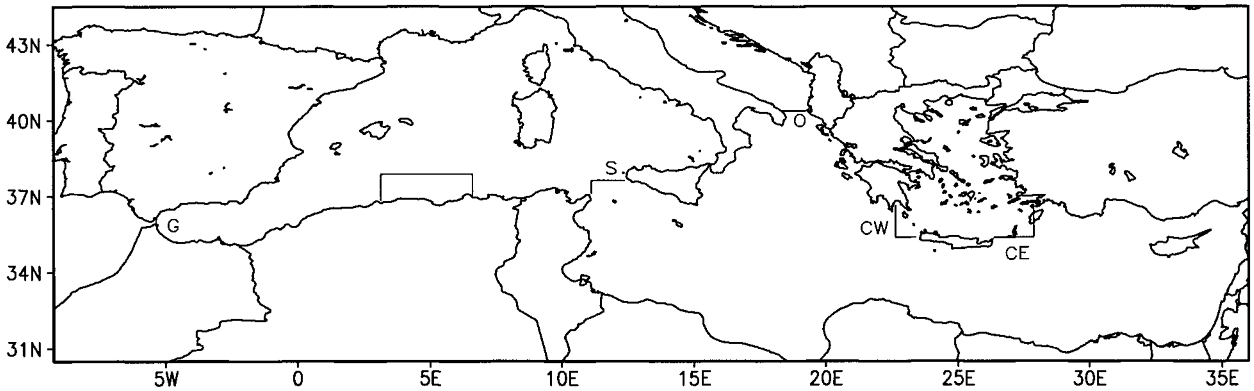

FIG. 13. Exact position of sections within the basin, used for the calculation of mass or heat transports (G, Straits of Gibraltar section; S, Sicily Strait section; O, Otranto Strait section; CE, eastern Cretan section; CW, western Cretan section). Also shown is the box area along the Algerian coast.

exactly equal but opposite in sign. However, when integrated up to z_0, the vertically integrated "barotropic" flow field contributes to the barotropic transport in each layer. Let us write the total horizontal velocity field as

$$\mathbf{v}_h = \mathbf{v}'_h + \overline{\mathbf{v}}_h \tag{14}$$

where $\mathbf{v}'_h$ is the baroclinic and $\overline{\mathbf{v}}_h$ is the barotropic part. Putting (14) into (13) we obtain

$$\text{total layer transport} = \int_{l_1}^{l_2}\int_{-H}^{z_o} \mathbf{v}'_h \hat{n}\, dz\, dl + \int_{l_1}^{l_2}\int_{-H}^{z_o} \overline{\mathbf{v}}_h \hat{n}\, dz\, dl. \tag{15}$$

Expanding the barotropic transport term (second term or the rhs of 15) we obtain

$$\int_{l_1}^{l_2}\int_{-H}^{z_o} \overline{\mathbf{v}}_h \hat{n}\, dz\, dl = \int_{l_1}^{l_2} \overline{\mathbf{v}}_h \cdot \hat{n}(z_o + H)\, dl = \int_{l_1}^{l_2} \frac{\partial(z_o + H)}{\partial l} \frac{\psi}{H}\, dl, \tag{16}$$

where ψ is the barotropic streamfunction. Thus the barotropic transport contribution in each layer is due to the slope of the interface across the section. The barotropic velocity field perpendicular to the section has the net effect of changing the position of that interface. We monitor both components of the layer transport, calling them baroclinic (first term on the rhs of 15) and barotropic (second term on the rhs of 15) transport components. In Fig. 14 we show the total AW layer transport (continuous curve) and its baroclinic component (dashed) for Gibraltar (panel a) and Sicily (panel b). Total and baroclinic transport appear to be almost identical for the Gibraltar case due to the fact that the meridional slope of the interface across Gibraltar is small because of the limited latitudinal extension of the strait. The transport there exhibits seasonal fluctuations (of the order of 0.1 Sv) around an average value of 0.93 Sv. Maximum transport is reached during September–October, which is in agreement with Ovchinnikov (1974) and Manzella and La Violette (1990) but not with Bormans et al. (1986).

At the Sicily Strait the situation changes since the total volume transport is very different from the simple baroclinic component. The barotropic contribution enhances the total layer transport so that the baroclinic transport is only 0.49 Sv on average while the total is 1.5 Sv on average. The total transport shows a large interannual signal that is mainly wind induced since it is due to the barotropic velocity component. At the Sicily Strait maximum transport is reached during December–January and minimum during May–June. With the exception of the winter of 1988, the Gibraltar transport is always leading by 2–3 months the Sicily transport as Manzella and La Violette (1990) conclude.

The net heat transport defined in (11) at Gibraltar (continuous line) and Sicily (dashed) for the central experiment is shown at Fig. 15. Positive values denote an eastward heat transport. The Gibraltar heat transport, which is always eastward, undergoes small seasonal fluctuations around an average of 2.7×10^{12} W. The Sicily heat transport on the other hand is mainly eastward (i.e., directed from the western to the eastern basin) but there are cases like in winters of 1981, 1987, and 1988 where it reverses for some time. It undergoes large seasonal fluctuations modulated by interannual frequencies (increased eastward heat transport during 1982 and 1987). The long-term average value (1.07×10^{13} W) compares very well with the 1.36×10^{13} W of heat advection that Bethoux (1979) estimates for the Sicily Strait. Transport maximum is reached during July–August while the minimum is during January–February. We note also a 1–2-month time lag between Gibraltar and Sicily heat transports with Gibraltar always leading. The peaks of heat transport occurring during the summers of 1982 and 1987 can be attributed to the response

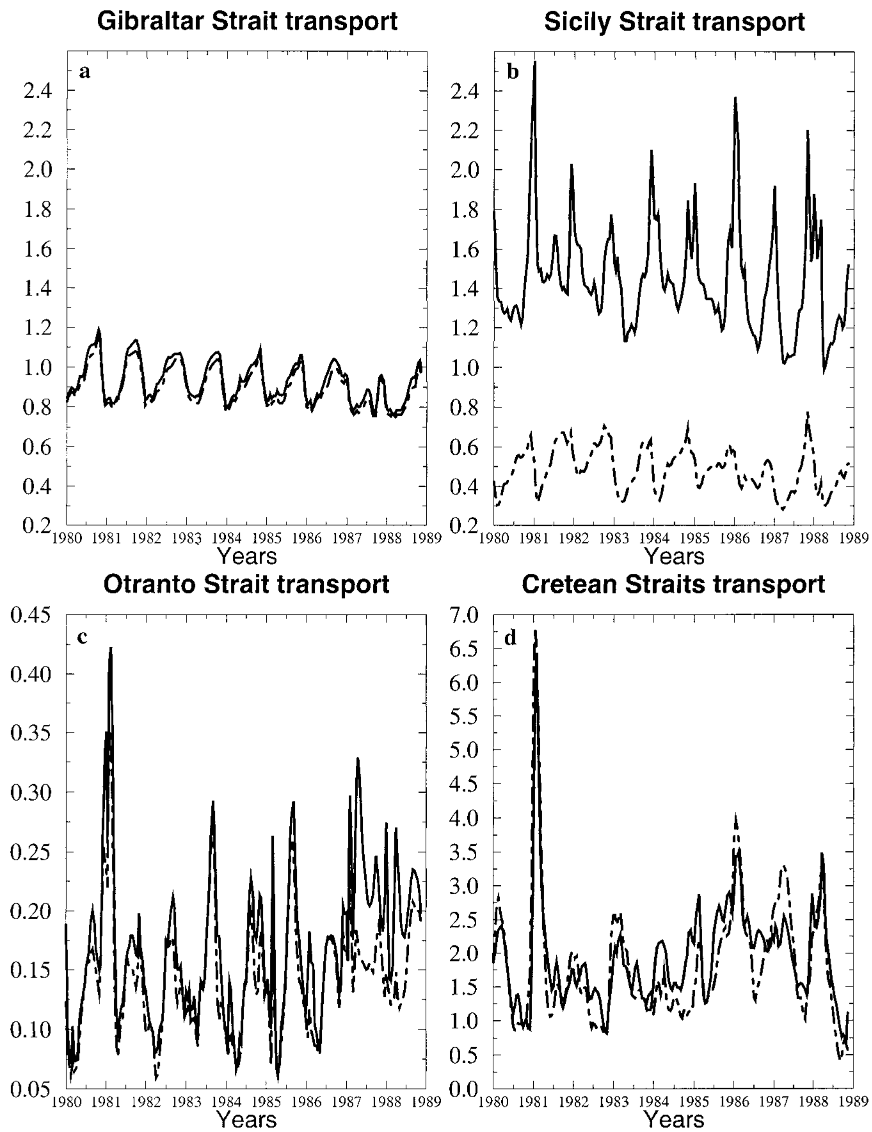

FIG. 14. (a) Gibraltar total (continuous line) and baroclinic mass transport, (b) Sicily total (continuous line) and baroclinic (dashed) mass transport, (c) Otranto total and baroclinic mass transport, and (d) eastern Cretan mass inflow to the Aegean (continuous line) and western Cretan mass outflow from the Aegean. The units are Sv. All figures refer to the central experiment.

of the EMED to the increased surface heat loss occurring there during the previous year (-9.96 W m^{-2} for 1981 and -9.39 W m^{-2} for 1986; see Table 3).

The northward (equal to the southward but with an opposite sign) baroclinic and barotropic volume transport at the Otranto Strait (sill depth $\sim$ 800 m), which connects the Ionian Basin with the Adriatic Sea, is shown in Fig. 14c (see also Fig. 13 for the position of the Otranto section). The total transport is slightly higher (0.17 Sv on average) than the baroclinic one with the differences becoming significant during the winter of 1981 and the period 1987–88. Both barotropic and baroclinic transports are seasonal with the total transport time series exhibiting semiseasonal and 2-yr interannual timescales. These periods are connected with double maxims occurring during January–February and August–October of 1981, 1983, 1985, and 1987 while the seasonality consists of a maximum achieved during August–October and a minimum during March–April. The intensified wind activity increases the water mass exchange at the strait with a global maximum of 0.42 Sv during January 1981. The second largest peak occurs during January–February 1987.

Finally in Fig. 14d we show the total mass inflow at the eastern Cretan section (CE in Fig. 13) into the Aegean and the mass outflow from the western Cretan section (CW in Fig. 13) being 1.94 and 1.84 Sv, respectively, on average. Notice also that there is no time

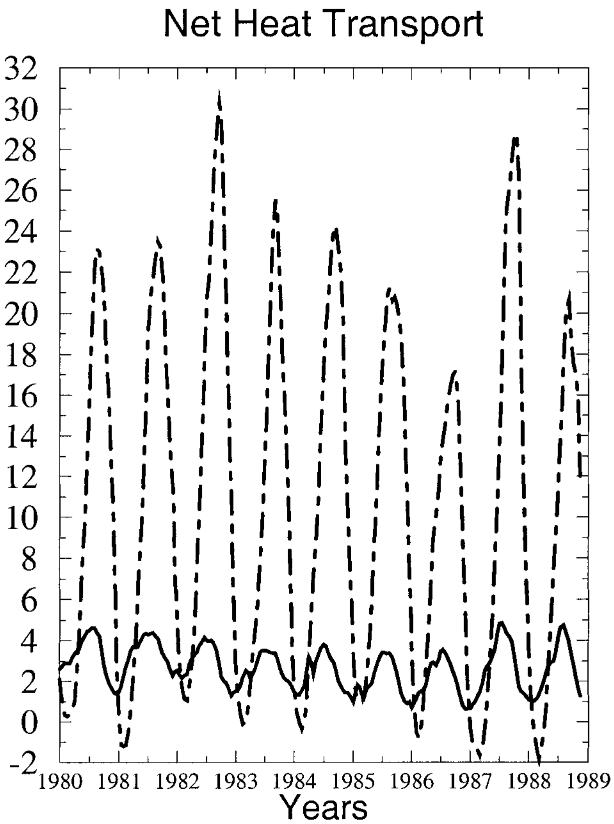

FIG. 15. Net heat transport at Gibraltar section (continuous line) and Sicily section vs time (1980–88, central expt). The units are W.

lag between the inflowing and outflowing waters from the Aegean. Maximum inflow/outflow is reached during January. We note also the existence of three anomalous peaks achieved during the winters of 1981, 1986, and 1988.

8. Model energetics

In this section the central, constant, and zero winds experiments (expts II and III in Table 2) are studied by means of an energy analysis scheme. This kind of analysis can highlight the role played by the external wind and themohaline forcing on the circulation.

We refer to barotropic (external mode) and baroclinic (internal mode) kinetic energy meaning the square of $\overline{\mathbf{v}}_h = (1/H)\int_{-H}^{0}\mathbf{v}_h\,dz$ and $\mathbf{v}'_h = \mathbf{v}_h - \overline{\mathbf{v}}_h$, respectively. The available potential energy (APE), baroclinic, and barotropic kinetic energy equations are now briefly discussed. The term APE, which goes back to Lorenz (1955), refers to the part of the potential energy that can be potentially transformed into kinetic energy through either the barotropic or baroclinic instability mechanisms.

Let us divide the pressure and density fields into a steady state (motionless) and a perturbation part:

$$p(x, y, z, t) = \tilde{p}(z) + p'(x, y, z, t) \quad \text{and} \tag{17}$$

$$\rho(x, y, z, t) = \tilde{\rho}(z) + \Delta(x, y, z, t). \tag{18}$$

The basic-state profiles $\tilde{p}(z)$, $\tilde{\rho}(z)$ can be estimated as long-term spatial averages of the pressure and density fields of the model integration.

Although the model solves for the temperature and salinity equations and the equation of state is nonlinear, we assume that the density is a linear function of T and S ($\Delta = \alpha T + \beta S$, $\alpha = \partial\rho/\partial T$, $\beta = \partial\rho/\partial S$). We thus neglect all pressure effects in density. This may be justified by knowing that the average bottom depth of the Mediterranean is only 1500 m and the main thermocline depth, where the energy conversions are larger (Pinardi and Robinson 1987), is only between 200 and 500 m. We can then write a density equation:

$$\begin{aligned}\frac{\partial\Delta}{\partial t} + \mathbf{v}_h\cdot\boldsymbol{\nabla}\Delta + w\frac{\partial\Delta}{\partial z} + w\frac{\partial\tilde{\rho}}{\partial z} &= -A_h\nabla^4\Delta + K_h\frac{\partial^2\Delta}{\partial z^2}\\ &\quad + [\alpha\gamma_T(T^* - T) + \beta\gamma_S(S^* - S)],\end{aligned} \tag{19}$$

where $\boldsymbol{\nabla}$ is the horizontal gradient operator and the term in brackets is derived from (4) and (5).

Multiplying (19) by $-g\Delta/s$, where $s = \partial\tilde{\rho}/\partial z$ is the basic stratification parameter, and taking into account the surface/bottom boundary conditions, we can derive an equation for the time rate of change of APE; that is,

$$\begin{aligned}\frac{\partial \mathrm{APE}}{\partial t} &= \boldsymbol{\nabla}\left(\mathbf{v}_h\frac{g\Delta^2}{2s}\right) + \frac{\partial}{\partial z}\left(\frac{wg\Delta^2}{2s}\right) + gw\frac{\partial s}{\partial z}\frac{\Delta^2}{2s^2}\\ &\quad + gw\Delta + AB + D_H + D_V,\end{aligned} \tag{20}$$

where $\mathrm{APE} = -g\Delta^2/2s$. The time rate of change of APE in (20) is due to the divergence of the horizontal/vertical transport of APE [first and second terms on the rhs of (20)], to the work done by the shear in the steady-state stability profile $SM = gw(\partial s/\partial z)(\Delta^2/2s^2)$, to the work done by the buoyancy forces $B = gw\Delta$, to the relaxation condition within the model Atlantic box $AB = -(g\Delta/s)[\alpha\gamma_T(T^* - T) + \beta\gamma_S(S^* - S)]$, and to the horizontal D_H and vertical D_V dissipation of APE; that is,

$$D_H = g\frac{\Delta}{s}A_h(\alpha\nabla^4 T + \beta\nabla^4 S) \quad \text{and}$$

$$D_V = -g\frac{\Delta}{s}K_h\left(\alpha\frac{\partial^2 T}{\partial z^2} + \beta\frac{\partial^2 S}{\partial z^2}\right).$$

Integrating (20) over the volume of the basin with the inclusion of the Atlantic box, we end up with the equation

$$\begin{aligned}\langle \mathrm{APE}_t\rangle &= \langle SM\rangle + \langle B\rangle + \langle SW\rangle + \langle AB\rangle + \langle D_H\rangle\\ &\quad + \langle D_V\rangle,\end{aligned} \tag{21}$$

where $\langle \cdot \cdot \cdot \rangle = (1/Vol) \iiint \cdot \cdot \cdot dV$ and Vol stands for the total volume of the basin. The surface buoyancy flux now appears in (21) due to the vertical diffusivities of temperature and salinity terms and it is written as $SW = -(g\Delta/s)[\alpha(\partial Q/\partial z) + \beta\gamma_S(S^* - S)]$.

Following Holland (1975), the normalized basin-integrated equations for the time rate of change of barotropic (external mode) $\langle \overline{E} \rangle = \langle \overline{\mathbf{v}}_h \cdot \overline{\mathbf{v}}_h/2 \rangle$ and baroclinic (internal mode) $\langle E' \rangle = \langle \mathbf{v}'_h \cdot \mathbf{v}'_h/2 \rangle$, and kinetic energy are (the basin is mechanically closed)

$$\langle \overline{E}_t \rangle = \langle N_e \rangle + \langle B_e \rangle + \langle W_e \rangle + \langle D_e \rangle \quad \text{and} \tag{22}$$

$$\langle E'_t \rangle = \langle N_i \rangle - \langle B \rangle - \langle B_e \rangle + \langle W_i \rangle + \langle D_i \rangle. \tag{23}$$

The analogous equation for the total kinetic energy is

$$\langle E_t \rangle = -\langle B \rangle + \langle W \rangle + \langle D \rangle. \tag{24}$$

Let us examine now the various terms appearing on the rhs of (22) and (23).

- $\langle N_e \rangle = -\langle \overline{\mathbf{v}}_h \cdot \overline{(\mathbf{v}_h \cdot \boldsymbol{\nabla}\mathbf{v}_h + w(\partial \mathbf{v}_h/\partial z))} \rangle$: Term $\langle N_e \rangle$ provides a mean of exchange between the two different reservoirs of kinetic energy through the action of nonlinear advective terms. For a mechanically closed basin (like in our case) it can be proved that $\langle N_e \rangle = -\langle N_i \rangle$ and this is the reason why no equivalent term appears in (24).
- $\langle B_e \rangle = -\langle (\overline{\mathbf{v}}_h \cdot \overline{\boldsymbol{\nabla} p} \rangle = -\langle (\overline{p} - p_b)\overline{\mathbf{v}}_h \cdot (\boldsymbol{\nabla} H/H) \rangle$ (where p_b is the pressure at the bottom): This is the conversion term of external mode kinetic energy to internal mode kinetic energy (or vice versa) through the divergence of pressure forces. We note also that this term comes from the JEBAR term in the barotropic momentum equation (Holland 1973; Huthnance 1984). In the flat bottom or homogeneous fluid case the term vanishes.
- The term $\langle B \rangle$, which appears with an opposite sign on the rhs of (21) and (23) [or (24)] is responsible for conversion of internal mode kinetic energy to APE (or vice versa) through the work done by buoyancy forces internal to the fluid.
- $\langle W_e \rangle = (1/Vol) \iint \overline{\mathbf{v}}_h \cdot \boldsymbol{\tau}_w \, dx\, dy$: This term corresponds to the time rate of change of barotropic kinetic energy due to the work done by the wind stress $\boldsymbol{\tau}_w$ at the surface. For the total kinetic energy the term takes the form $\langle W \rangle = (1/Vol) \iint \mathbf{v}_h \cdot \boldsymbol{\tau}_w \, dx\, dy$ while for the internal kinetic energy it is simply $\langle W_i \rangle = \langle W \rangle - \langle W_e \rangle$.
- The term $\langle D_e \rangle$ corresponds to the loss of barotropic kinetic energy due to the dissipative forces in horizontal and vertical; that is, $\langle D_e \rangle = \langle D_{eh} \rangle + \langle D_{eV} \rangle$. The term $\langle D_{eV} \rangle$ vanishes in our case since the bottom friction $\boldsymbol{\tau}_b$ is set to zero while $\langle D_{eh} \rangle = -A_m \langle \overline{\mathbf{v}}_h \cdot \overline{\nabla^4 \mathbf{v}}_h \rangle$.
- The loss of baroclinic kinetic energy $\langle D_i \rangle$ can be written as $\langle D_i \rangle = \langle D_{ih} \rangle + \langle D_{iV} \rangle$, where $\langle D_{ih} \rangle = -A_m \langle \mathbf{v}_h \cdot \nabla^4 \mathbf{v}_h - \overline{\mathbf{v}}_h \cdot \overline{\nabla^4 \mathbf{v}} \rangle$ and $\langle D_{iV} \rangle = -K_m \langle (\partial^2 \mathbf{v}_h/\partial z^2)^2 \rangle$ (since $\boldsymbol{\tau}_b = 0$). The energy analysis was performed offline, using the model snapshots every 15 days for the whole period of integration. Both $\langle \overline{E}_t \rangle$ and $\langle E'_t \rangle$ were calculated by summing up the terms appearing on the rhs of (22) and (23), respectively. However in the APE equation (21), the offline calculation of term $\langle D_V \rangle$ is not done taking into account the parameterization of convective adjustment so the time rate of change of APE cannot be estimated.

The exchanges taking place between the three distinct energy reservoirs are presented here as long-term averages over the first 8 yr of interannual integration of the model (1980–87). The box diagrams in Figs. 16a–c show the energy cycle corresponding to the central and experiments II and III.

In the central experiment the internal mode is driven by the work done by the wind alone while 62% of the energy received is transferred to APE through the action of the buoyancy forces. Lateral and interior friction dissipate 18.7% of the energy received (bottom friction is zero) while there is some small leakage (3.1%) to external mode energy due to the nonlinear advective terms.

The external mode kinetic energy on the other hand receives almost equal contributions by the wind action and the conversion of internal mode kinetic energy through the work done by pressure forces (48.2% and 44.4%, respectively, of the total energy received) while 89.5% of the energy is dissipated by lateral friction (interior and bottom friction are identically zero). Overall, the wind energy is mainly received by the internal mode while the most vigorous kinetic energy dissipation is done by lateral friction acting on the external mode.

The APE reservoir receives energy mainly from the action of the thermohaline fluxes at the surface (61% of the total energy received) while the conversion of interal mode kinetic energy contributes 21%. Dissipation of available potential energy is mainly due to vertical diffusive effects $\langle D_V \rangle$ and as we have already pointed out, the term $\langle D_V \rangle$ is underestimated since we miss the part due to the convective adjustment process of the model. The terms $\langle AB \rangle$ and $\langle SM \rangle$ contribute 12.4% and 4%, respectively, to the total available potential energy received. The normalized volume integrated mean of kinetic and available potential energy over the first 8 yr of integration are shown in first column of Table 4. Knowing that the ratio $\langle \mathrm{APE} \rangle / \langle E \rangle \sim L^2/L_D^2$ (Pedlosky 1987), we derive that the energy is stored at scales of motion $L \sim 16$ times larger than the Rossby deformation radius L_D.

In the constant winds experiment (expt II), the direction of the energy flow remains the same as before. The main characteristics of the energy cycle of this experiment are the following.

1) The standard deviations of the terms entering the internal and external mode kinetic energy equations have been greatly reduced with respect to the central experiment due to the zero variability of the wind forcing.
2) The long-term mean behavior of the baroclinic and APE equations terms is almost unaffected by the absence of wind forcing variability. The internal

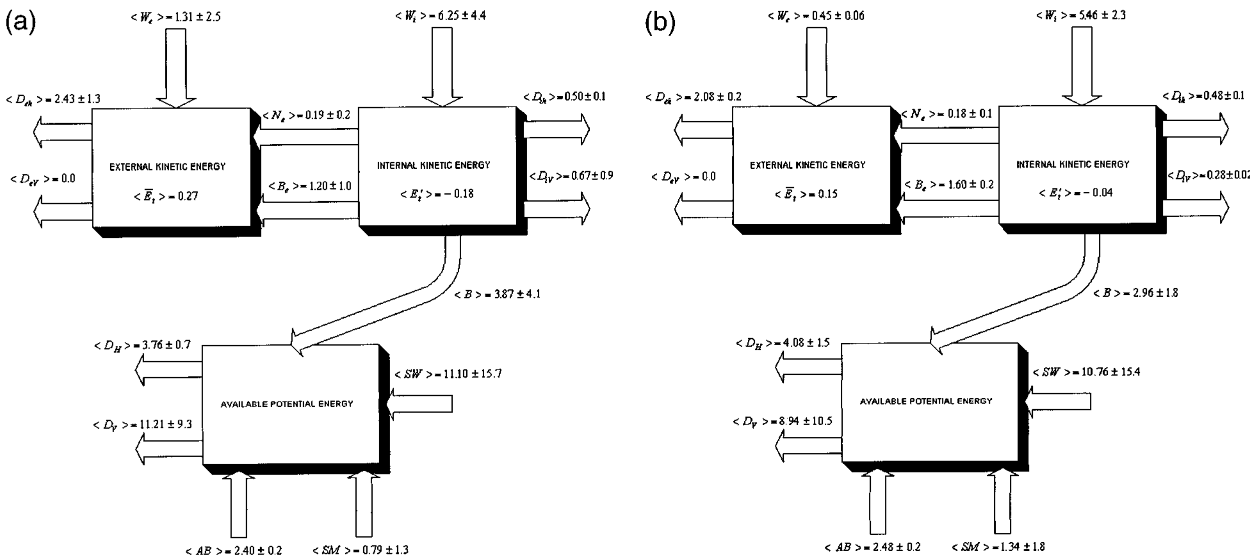

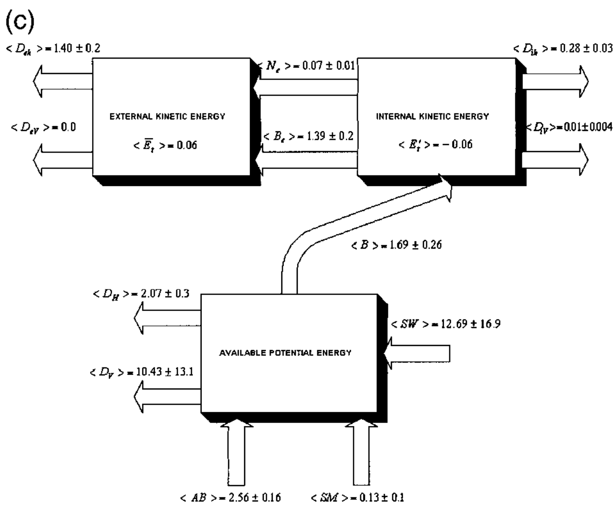

FIG. 16. Energy cycle corresponding to (a) the central, (b) the constant winds (expt II), and (c) the zero winds (expt III) experiments averaged over the period 1980–88. Arrows show direction of energy flow while for each term its mean value and standard deviation are shown. Units are 10^{-6} erg cm^{-3} s.

mode kinetic energy is driven by the constant wind forcing alone while 54% of the total energy received is converted to APE and 14% is dissipated through the action of lateral and interior friction. Available potential energy is provided by the thermohaline fluxes at the surface (61% of the total energy received) and by the conversion of internal kinetic energy (17%). The main sink of APE is again due to vertical diffusive effects (although underestimated).

3) External mode kinetic energy is the quantity that is more sensitive to the absence of wind forcing variability. The energy provided to the external mode by the wind forcing has been greatly reduced with respect to the central experiment, contributing now 20.3% to the total barotropic kinetic energy. On the other hand the conversion of internal kinetic energy through the work done by pressure forces dominates in this case, contributing 71.6% of the total energy. The dissipation of barotropic energy is again due to lateral friction. The external mode kinetic energy has a net increasing trend with a time rate equal to 0.15 $\times 10^{-6}$ erg cm^{-3} s^{-1}. The overall mean total kinetic energy of this experiment (Table 4, second column) has decreased with respect to the central experiment while the value of APE remains almost the same.

TABLE 4. Normalized basin-integrated total kinetic and available potential energy for central expt and expts II and III.

	Central	Expt II	Expt III
$\langle E\rangle$	2.13 ergs cm^{-3}	1.62 ergs cm^{-3}	0.71 ergs cm^{-3}
$\langle APE\rangle$	525.18 ergs cm^{-3}	531.34 ergs cm^{-3}	543.02 ergs cm^{-3}

The energy cycle of the zero winds experiment (expt III; Table 2) is characterized by the reversal of the conversion between internal mode kinetic energy and APE since the wind action does not provide any more energy to the internal mode. The external mode is driven now exclusively by the conversion of internal mode kinetic energy due the work done by the pressure forces. In Table 4 we show that kinetic energy is now decreased by 65% or more with respect to central experiment. This shows that the wind is responsible for about 70% of the general circulation kinetic energy, a classical textbook result for the remaining ocean basins.

The energy cycle of the Mediterranean Sea general circulation in response to low-frequency atmospheric variability can be summarized as follows.

- Wind input triggers an inverse baroclinic cascade of energy from baroclinic kinetic to potential energy. The barotropic mode kinetic energy is dissipated by lateral viscosity terms and it is the major sink of energy for the general circulation.
- In the absence of winds (likewise for summer or weak interannual forcing conditions) the energy is mainly transferred by buoyancy work from APE to kinetic energy following a direct baroclinic energy cascade, typical of nonlinear baroclinic instability processes.
- The nonlinear advection and pressure work terms convert energy from the baroclinic to the barotropic mode. This energy transfer will reinforce the tendency of the general circulation to transfer energy from smaller to larger spatial scales, a process known to be typical of two-dimensional quasigeostrophic turbulence.

Thus we argue that the Mediterranean Sea general circulation is storing energy during winter (and more during the anomalous winter events described in this paper) in the density field while it releases it to the horizontal circulation during summer. We believe this result is similar to what obtained for the North Atlantic general circulation (Holland 1975). The energy conversion terms also give us the key to understand the memory of the system mechanism. If we look at the buoyancy conversion term year by year we find that 1981 and 1986 had absolute and relative maxima, respectively, for the 1980–88 period. This means that these anomalous winters store more APE than others and thus enhance the memory of the general circulation. Thus information in the form of APE is stored more efficiently during the winters of 1981 and 1986, which is complementary to the finding that a deep mixed layer is an indicator of storage of winter cooling in deeper layers.

9. Comparison with observations

The general circulation surveys of the POEM Group (1992) offer the opportunity to compare the dynamic height fields produced in the central experiment and the observational evidence. In Fig. 17 we compare the dynamic height fields at 300 m for the periods October–November 1985 (panel a) and March–April 1986 (panel b) with the analyses done by Ozsoy et al. (1993). In Fig. 18 we show the comparison with the September 1987 data analysis of Robinson et al. (1991). A new synthesis of 1987 observational data has been done by Malanotte-Rizzoli et al. (1997), which confirms the observational picture of Robinson et al. (1991).

It is apparent from almost all intercomparison we present that the model is capable reproducing some of the large-scale structure of jets and gyres in the eastern basin revealed by the observations.

On the other hand the vigorous eddy field, present especially in the Levantine area, which interacts with and subsequently modifies the mean flow driven by the atmospheric parameters, is not resolved by our model, so many scales of the observational flow field are still missing from the simulations. Furthermore we argue that some of the missing features like the strong Mersa–Matruh gyre in Fig. 17b) could be due to inaccuracies in the atmospheric forcing.

During October–November 1985 the area of intercomparison is confined east of the Cretan passage. The Rhodes and Mersa–Matruh gyres are somehow reproduced by the model but features are shifted and the Shikmona complex of gyres is missing. Furthermore the Antalya anticyclone is absent. We can speculate that direct atmospheric forcing is responsible for some of the large-scale features of the Rhodes gyre (since we cannot get these structures by the constant wind or no wind experiment) but the eddy signal is also very relevant.

During the winter of 1986 (March–April) the model produces a rather strong and extended Rhodes gyre pushing the MMJ to flow along the African coast. The Mersa–Matruh gyre then disappears even if it is present in the observations. The model shows some skill in reproducing the anticyclonic field south of Cyprus. It is also interesting that now we get a clear signature of the Antalya anticyclone present in the observational field. The most striking model/observations intercomparison is the one of September 1987. This particular survey offers the most extended hydrographic coverage in the EMED. The northward extension of the Atlantic–Ionian stream as well as the elongated Rhodes and the strong Mersa–Matruh gyres are well captured by the model simulation. The model is also reproducing the anticyclonic motion (Shikmona gyre) in the southeastern Levantine but the eddy signal evident in the observations is clearly missing. The MMJ, interconnecting the flow field between the Ionian and Levantine Basins, appears as a smooth and well-defined structure in our simulation while the observations show more jet segments than a unique flow structure. This model data intercomparison, the first of this kind to be carried out with a GCM, was made possible by the rather unusual extension in space and time of the POEM dataset. We can argue that some of the features reproduced by the model are due to the specific forcing used, which means they are directly driven by the atmospheric forcing.

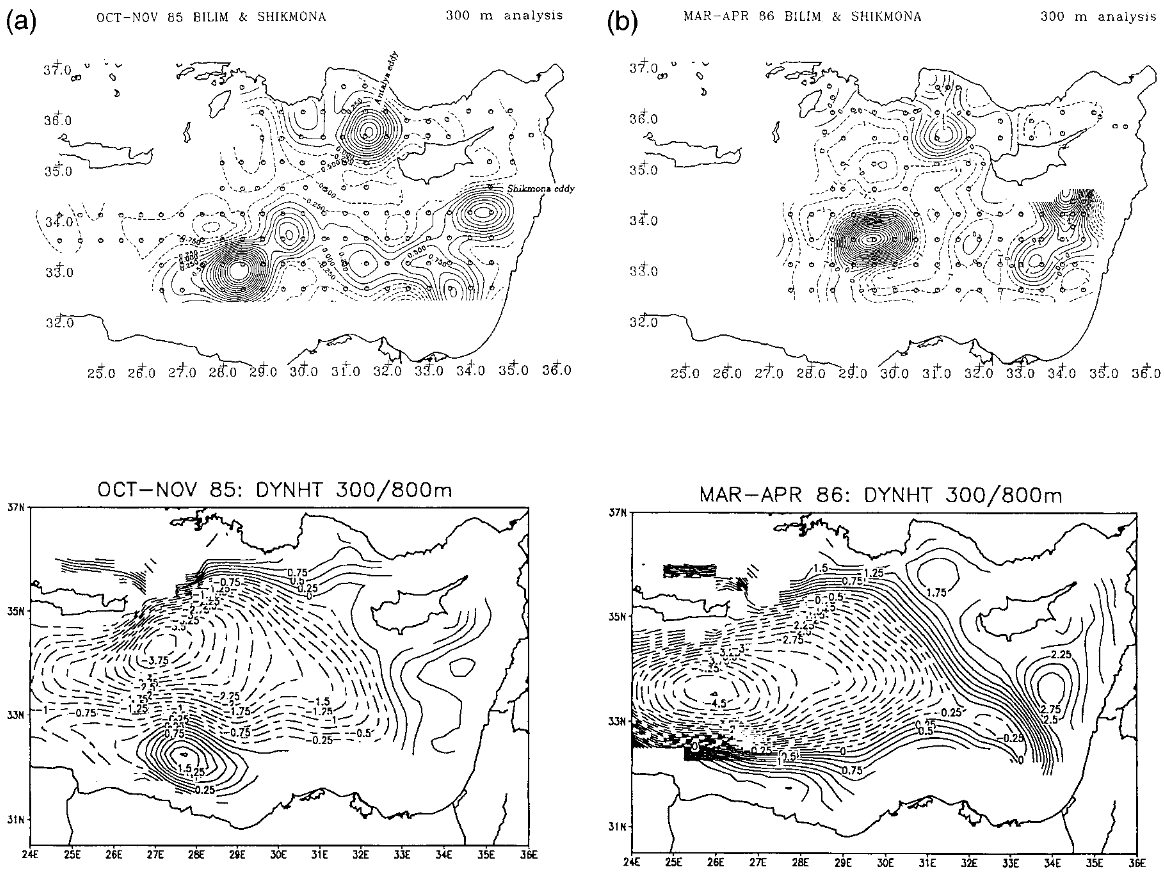

FIG. 17. (a) Dynamic height anomaly contours for Oct–Nov 1985 from the POEM data (Ozsoy et al. 1993) (upper panel) and the central expt of the model (lower panel) at 300 m. (b) Dynamic height anomaly contours for Mar–Apr 1986 from the POEM data (Ozsoy et al. 1993) (upper panel) and the central expt of the model (lower panel) at 300 m. The units are cm and the reference level is at 800 m.

10. Conclusions

In this work we have studied the Mediterranean general circulation response to the atmospheric forcing for the period 1980–88. The low-frequency atmospheric variability over the Mediterranean creates seasonal and interannual anomalies in the heat and momentum budgets at the air–sea interface. This in turn produces large ocean circulation changes at both seasonal and interannual timescales. The interannual response of the basin is amplified in the EMED where local and remote wind forcing winter anomalies are ''memorized'' and the upcoming seasonal cycle changed. The highly anomalous winters of 1981 and 1986 trigger an altered oceanic response that drives the upcoming summer flow field variability and the next winter current pattern. We have shown that after these strong cyclonic vorticity (curl) input events the basin currents are modified up to a year later. It remains to be shown if a threshold exists to this capability of shifting the seasonal cycle after an anomalous winter wind curl event.

We have shown evidence that the winter circulation conditions constitute a necessary ingredient for the summer circulation structure. The winter mixed layer helps the surface information to be carried all the way down to thermocline depths and thus sets the memory of the basin, which is going to specify then the response in the summer period that follows. This mechanism is found to be locked to the wind anomalies of the winter period, which sets the circulation characteristics capable of modifying the upcoming seasonal cycle. Although this is a first strong indication of the interaction between seasonal and interannual timescales the whole concept calls for further experimentaiton and understanding.

The strongest interannual variability is localized at intermediate depths (LIW layer) and in areas like the eastern Levantine (area of LIW production) and the Ionian. The interannual response is gyrelike in general but also involves paths and strengths of free and boundary currents in the basin. In the WMED a regular seasonal cycle overwhelms interannual changes of the circulation probably due to the limited extension of the deep mixed layer areas.

The existence and strength of the Algerian undercurrent is found to be linked to the amplitude and polarity of the curl of the wind stress over the WMED. Whenever the wind curl reaches very high positive val-

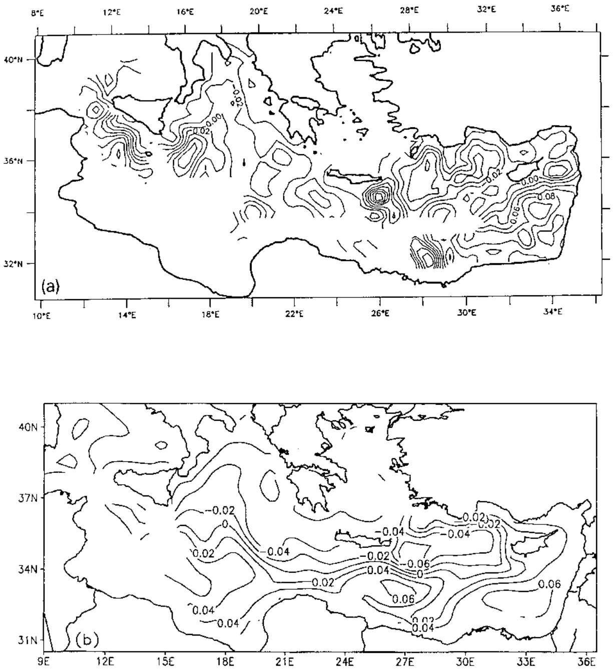

FIG. 18. Dynamic height anomaly contours for Sep 1987 at 30 m (reference level 450 m). (a) POEM data (Robinson et al. 1991) and (b) from the central expt of the model. The units are m.

ues (this can usually happen during the winter period), the undercurrent weakens or even disappears. In those cases the LIW transport west of Sardinia is exclusively due to the northward branch that flows along the western coast of Sardinia.

An important interannual variability index is the mass transport at the various straits of the basin. In particular the mass transports at the Straits of Gibraltar and the Sicily Strait is consistent with a number of observations both in value and in phase. The Gibraltar volume transport undergoes small seasonal changes around an average value of 0.93 Sv and the Sicily volume transport exhibits large seasonal and interannual fluctuations around an average of 1.5 Sv. We believe we have explained for the first time why the interannual fluctuations at Sicily are due to the wind effects and that correct estimates of Sicilian volume transports could be done with only current meter measurements.

Although the model forms a kind of LIW water, it is unable to reproduce the deep Mediterranean waters either in the WMED (Gulf of Lions) or in the EMED (southern Adriatic). Recent results have shown that tuning of the air–sea physical parameterizations and higher-frequency atmospheric forcing could be important to trigger deep convection in our model. However further research is needed before the issue of deep waters in a GCM can be settled.

Last, we have shown that the energy cycle of the basin involves transfer of kinetic energy into available potential energy in the presence of the low-frequency wind forcing, while the reverse is true for the case of no wind. This last case corresponds to having a baroclinic conversion mechanism acting on the general circulation, which is typical of baroclinic instability processes. This could offer a first explanation for the different intensity of the mesoscale eddy field in certain parts of the basin (Ayoub et al. 1998).

Acknowledgments. This work has been supported by the EU-MAST Contract MERMAIDS (MAST-CT90-0039 and MAST2-C93-0055). The first author was supported by EU-MAST Contract B/MAST 913005. The last part of the work has been supported by the EU/MAST MATER project (Contract MAS3-CT96-0051) and MFSPP EU-MAST (MAS3-CT98-0171). We would like to express our gratitude to Dr. S. Castellari, Dr. A. Navarra, Dr. M. Zavatarelli, and the MERMAIDS group for their invaluable and stimulating critiques to the work. We also thank Mr. Paolo Carini, Mr. Leonidas Perivoliotis, and Miss Elisabetta Masetti for helping us with data mapping.

REFERENCES

Astraldi, M., C. N. Bianchi, and C. Morri, 1994: Climatic fluctuations, current variability and marine species distribution: A case study in the Ligurian Sea (northwest Mediterranean). *Oceanol. Acta,* **18,** 139–149.

Ayoub, N., P.-Y. Le Traon, and P. De Mey, 1998: A description of the Mediterranean surface variable circulation from combined ERS-1 and Topex/Poseidon altimetric data. *J. Mar. Syst.,* **18,** 3–40.

Bethoux, J. P., 1979: Budgets of the Mediterranean Sea. Their dependence on the local climate and on the characteristics of the Atlantic waters. *Oceanol. Acta,* **10,** 157–163.

——, and B. Gentili, 1996: The Mediterranean Sea, coastal and deep-sea signatures of climatic and environmental changes. *J. Mar. Syst.,* **7,** 383–394.

Bormans, M., C. Garrett, and K. R. Thompson, 1986: Seasonal variability of the surface inflow through the Strait of Gibraltar. *Oceanol. Acta,* **9,** 403–414.

Brasseur, P., J. M. Brankart, J. M. Beckers, and R. Schoenauen, 1996: Seasonal temperature and salinity fields in the Mediterranean Sea: Climatological analyses of an historical data set. *Deep-Sea Res.,* **43,** 159–192.

Bryden, H. L., and T. H. Kinder, 1990: Steady two-layer exchange through the Strait of Gibraltar. *Deep-Sea Res.,* **38** (Suppl. 1), S445–S463.

Castellari, S., N. Pinardi, and K. D. Leaman, 1998: A model study of air–sea interactions in the Mediterranean Sea. *J. Mar. Sys.,* **18,** 89–114.

Cressman, G. P., 1959: An operational objective analysis system. *Mon. Wea. Rev.,* **87,** 367–374.

Garrett, C., R. Outerbridge, and K. Thompson, 1993: Interannual variability in Mediterranean heat and buoyancy fluxes. *J. Climate,* **6,** 900–910.

Haines, K., and P. Wu, 1995: A modelling study of the thermocline circulation of the Mediterranean Sea: Water formation and dispersal. *Oceanol. Acta,* **18,** 401–417.

Heburn, G. W., 1994: The dynamics of the seasonal variability of the western Mediterranean circulation. *Coastal Estuarine Stud.,* **46,** 249–285.

Hecht, A., 1992: Abrupt changes in the characteristics of Atlantic and Levantine Intermediate Waters in the southeastern Levantine Basin. *Oceanol. Acta,* **15,** 25–42.

Hellerman, S., and M. Rosenstein, 1983: Normal monthly wind stress

over the world ocean with error estimates. *J. Phys. Oceanogr.,* **17,** 158–163.
Herbaut, C., L. Mortier, and M. Crepon, 1996: A sensitivity study of the general circulation of the western Mediterranean. Part I: The response to density forcing through the straits. *J. Phys. Oceanogr.,* **26,** 65–84.
——, ——, and ——, 1997: A sensitivity study of the general circulation of the western Mediterranean. Part II: The response to atmospheric forcing. *J. Phys. Oceanogr.,* **27,** 2126–2145.
Holland, W. R., 1973: Baroclinic and topographic influences on the transport in western boundary currents. *Geophys. Fluid Dyn.,* **4,** 187–210.
——, 1975: Energetics of baroclinic motions. *Numerical Models of the Ocean Circulation,* National Academy of Sciences, 168–177.
Horton, C., M. Clifford, J. Schmitz, and L. H. Kantha, 1997: A real-time oceanographic nowcast/forecast system for the Mediterranean Sea. *J. Geophys. Res.,* **102** (C11), 25 123–25 156.
Huthnance, J. M., 1984: Slope currents and ''JEBAR.'' *J. Phys. Oceanogr.,* **14,** 795–810.
Korres, G., N. Pinardi, and A. Lascaratos, 2000: The ocean response to low-frequency interannual atmospheric variability in the Mediterranean Sea. Part II: Empirical orthogonal functions analysis. *J. Climate,* **13,** 732–745.
Lacombe, H., and C. Richez, 1982: The regime of the Strait of Gibraltar. *Hydrodynamics of Semienclosed Seas,* J. C. J. Nihoul, Ed., Elsevier, 13–74.
Lascaratos, A., and K. Nittis, 1998: A high-resolution three-dimensional numerical study of Intermediate Water formation in the Levantine Sea. *J. Geophys. Res.,* **103** (C9), 18 497–18 511.
——, R. Williams, and E. Tragou, 1993: A mixed-layer study of the formation of Levantine Intermediate Water. *J. Geophys. Res.,* **98,** 14 739–14 749.
Leaman, K. D., and F. A. Schott, 1991: Hydrographic structure of the convection regime in the Gulf of Lions: Winter 1987. *J. Phys. Oceanogr.,* **21,** 575–598.
Lorenz, E. N., 1955: Available potential energy and the maintenance of the general circulation. *Tellus,* **7,** 157–167.
Lowe, P. R., 1977: An approximating polynomial for the computation of the saturation water pressure. *J. Appl. Meteor.,* **16,** 100–103.
Madec, G., M. Chartier, P. Delecluse, and M. Crepon, 1991: A three-dimensional numerical study of deep-water formation in the northwestern Mediterranean Sea. *J. Phys. Oceanogr.,* **21,** 1349–1371.
Malanotte-Rizzoli, P., and A. Bergamasco, 1991: The wind and thermally driven circulation of the eastern Mediterranean Sea. Part II: The baroclinic case. *Dyn. Atmos. Oceans,* **15,** 179–214.
——, and Coauthors, 1997: A synthesis of the Ionian Sea hydrography, circulation and water mass pathways during POEM-Phase I. *Progress in Oceanography,* Vol. 39, Pergamon Press, 153–204.
Manzella, G. M. R., and P. E. LaViolette, 1990: The seasonal variation of water mass content in the Western Mediterranean and its relationship with the inflows through the Straits of Gibraltar and Sicily. *J. Geophys. Res.,* **95,** 1623–1626.
Milliff, R. F., and A. R. Robinson, 1992: Structure and dynamics of the Rhodes gyre system and dynamical interpolation for estimates of the mesoscale variablity. *J. Phys. Oceanogr.,* **22,** 317–337.
Millot, C., 1991: Mesoscale and seasonal variabilities of the circulation in the western Mediterranean. *Dyn. Atmos. Oceans,* **15,** 179–214.
——, 1994: Models and data: A synergetic approach in the Western Mediterranean. *Ocean Processes in Climate Dynamics: Global and Mediterranean Examples,* P. Malanotte-Rizzoli and A. R. Robinson, Eds., NATO ASI Series, Vol. C 419, 407–425.
Myers, P., K. Haines, and S. Josey, 1998: On the importance of the choice of wind stress forcing to the modelling of the Mediterranean Sea circulation. *J. Geophys. Res.,* **103,** 15 729–15 749.
Ozsoy, E., 1981: On the atmospheric factors affecting the Levantine Sea. European Centre for Medium-Range Forecasts Tech. Rep. 25, 29 pp.
——, A. Hecht, U. Unluata, S. Brenner, H. I. Sur, J. Bishop, M. A. Latif, Z. Rozentraub, and T. Oguz, 1993: A synthesis of the Levantine basin circulation and hydrography, 1985–1990. *Deep-Sea Res., II,* **40,** 1075–1119.
Ovchinnikov, I. M., 1966: Circulation in the surface and intermediate layers of the Mediterranean. *Oceanology,* **6,** 48–59.
——, 1974: On the water balance of the Mediterranean Sea. *Oceanology,* **14,** 198–202.
Pacanowski, R. C., K. Dixon, and A. Rosati, 1991: Princeton University, GFDL Ocean Group Tech Rep. 2, 46 pp.
Pedlosky, J., 1987: *Geophysical Fluid Dynamics.* Springer-Verlag, 710 pp.
Pinardi, N., and A. R. Robinson, 1987: Dynamics of deep thermocline jets in the POLYMODE region. *J. Phys. Oceanogr.,* **17,** 1163–1188.
——, and A. Navarra, 1993: Baroclinic wind adjustment processes in the Mediterranean Sea. *Deep-Sea Res. II,* **40,** 1299–1326.
——, G. Korres, A. Lascaratos, V. Roussenov, and E. Stanev, 1997: Numerical simulation of the Mediterranean Sea upper ocean circulation. *Geophys. Res. Lett.,* **24,** 425–428.
POEM Group, 1992: General circulation of the eastern Mediterranean. *Earth Sci. Rev.,* **32,** 285–309.
Robinson, A. R., and M. Golnaraghi, 1993: Circulation and dynamics of the eastern Mediterranean Sea: Quasi-synoptic data-driven simulations. *Deep-Sea Res. II,* **40,** 1207–1246.
——, and Coauthors, 1991: Structure and variability of the eastern Mediterranean general circulation. *Dyn. Atmos. Oceans,* **15,** 215–240.
Roether, W., B. B. Manca, B. Klein, D. Bregant, D. Georgopoulos, V. Beitzel, V. Kovacevic, and A. Luchetta, 1996: Recent changes in eastern Mediterranean deep waters. *Science,* **271,** 333–335.
Rosati, A., and K. Miyakoda, 1988: A general circulation model for upper ocean circulation. *J. Phys. Oceanogr.,* **18,** 1601–1626.
Roussenov, V., E. Stanev, V. Artale, and N. Pinardi, 1995: A seasonal model of the Mediterranean Sea general circulation. *J. Geophys. Res.,* **100,** 13 515–13 538.
Tziperman, E., and P. Malanotte-Rizzoli, 1991: The climatological seasonal circulation of the Mediterranean. *J. Mar. Res.,* **49,** 1–25.
Wu, P., and K. Haines, 1996: Modeling the dispersal of Levantine Intermediate Water and its role in Mediterranean deep water formation. *J. Geophys. Res.,* **101,** 6591–6607.
Wust, G., 1961: On the vertical circulation of the Mediterranean Sea. *J. Geophys. Res.,* **66,** 3261–3271.
Zavatarelli, M., and G. L. Mellor, 1995: A numerical study of the Mediterranean Sea circulation. *J. Phys. Oceanogr.,* **25,** 1384–1414.